

1 **Properties of Glial Cell at the Neuromuscular Junction are Incompatible with synaptic**
2 **repair in the SOD1^{G37R} ALS mouse model**

3 Martineau Éric^{1,2}, Danielle Arbour^{1,2}, Joanne Vallée^{1,2}, Robitaille Richard^{1,2*}.

4 Abbreviated title: Unfit glial repair properties at the NMJ in ALS

5 ¹: Département de neurosciences, Université de Montréal, PO box 6128, Station centre-ville,
6 Montréal, Québec, Canada, H3C 3J7

7 ²: Groupe de recherche sur le système nerveux central, Université de Montréal.

8 * : To whom correspondence should be addressed : richard.robitaille@umontreal.ca, Université
9 de Montréal, PO box 6128, Station centre-ville, Montréal, Québec, Canada, H3C 3J7

10 Number of pages: 46

11 Number of figures: 9

12 Number of tables: 1

13 Numbers of words in the abstract: 246/250

14 Numbers of words in the introduction: 686/650

15 Numbers of words in the discussion: 1963/1500

16 **Conflict of interest:** The authors declare no competing financial interests.

17 **Acknowledgements:** This work was funded by grants from the Canadian Institutes for Health
18 Research (R.R. MOP-111070), Robert Packard Center for ALS Research (R.R.), Canadian
19 Foundation for Innovation (R.R), and an infrastructure grant from the Fonds Recherche Québec-
20 Santé Leader Opportunity Fund to the GRSNC. É.M. held a doctoral studentship from the ALS
21 Society of Canada and a master's degree studentship from the Fonds Recherche Québec-Santé.
22 We thank Félix-Antoine Robert for help regarding the statistical analysis.

1 **ABSTRACT**

2 Amyotrophic lateral sclerosis (ALS) is a fatal neurodegenerative disease affecting
3 motoneurons in a motor-unit (MU) dependent manner. Glial dysfunction contributes to numerous
4 aspects of the disease. At the neuromuscular junction (NMJ), early alterations in perisynaptic
5 Schwann cell (PSC), glial cells at this synapse, may impact their ability to regulate NMJ stability
6 and repair. Indeed, muscarinic receptors (mAChR) regulate the repair phenotype of PSCs and are
7 overactivated at disease-resistant NMJs (*Soleus* muscle) in SOD1^{G37R} mice. However, it remains
8 unknown whether this is the case at disease-vulnerable NMJs and whether it translates into an
9 impairment of PSC-dependent repair mechanisms. We used *Soleus* and *Sternomastoid* muscles
10 from SOD1^{G37R} mice and performed Ca²⁺-imaging to monitor PSC activity and used
11 immunohistochemistry to analyze their repair and phagocytic properties. We show that PSC
12 mAChR-dependent activity was transiently increased at disease-vulnerable NMJs (*Sternomastoid*
13 muscle). Furthermore, PSCs from both muscles extended disorganized processes from
14 denervated NMJs and failed to initiate or guide nerve terminal sprouts at disease-vulnerable
15 NMJs, a phenomenon essential for compensatory reinnervation. This was accompanied by a
16 failure of numerous PSCs to upregulate Galectin-3 (MAC-2), a marker of glial axonal debris
17 phagocytosis, upon NMJ denervation in SOD1 mice. Finally, differences in these PSC-dependent
18 NMJ repair mechanisms were MU-type dependent, thus reflecting MU vulnerability in ALS.
19 Together, these results reveal that neuron-glia communication is ubiquitously altered at the NMJ
20 in ALS. This appears to prevent PSCs from adopting a repair phenotype, resulting in a
21 maladapted response to denervation at the NMJ in ALS.

22
23
24

1 **SIGNIFICANCE STATEMENT**

2 Understanding how the complex interplay between neurons and glial cells ultimately lead to the
3 degeneration of motor neurons and loss of motor function is a fundamental question to
4 comprehend amyotrophic lateral sclerosis. An early and persistent alteration of glial cell activity
5 takes place at the neuromuscular junction (NMJ), the output of motor neurons, but its impact on
6 NMJ repair remains unknown. Here, we reveal that glial cells at disease-vulnerable NMJs often
7 fail to guide compensatory nerve terminal sprouts and to adopt a phagocytic phenotype on
8 denervated NMJs in SOD1^{G37R} mice. These results show that glial cells at the NMJ elaborate an
9 inappropriate response to NMJ degeneration in a manner that reflects motor-unit vulnerability
10 and potentially impairs compensatory reinnervation.

11

12

1 INTRODUCTION

2 Amyotrophic lateral sclerosis (ALS) is a neurodegenerative disease characterized by the
3 progressive loss of motoneurons (MNs), with fast-fatigable (FF) motor-units (MUs) being more
4 vulnerable than fast-fatigue-resistant (FR) and slow (S) MUs (Frey et al., 2000; Pun et al., 2006;
5 Hegedus et al., 2007; Hegedus et al., 2008). Over the last decade, evidence of disease onset and
6 progression being modulated by numerous non-cell autonomous mechanisms has highlighted the
7 importance of glial cells in this disease (Boillee et al., 2006a; Ilieva et al., 2009; Kang et al.,
8 2013; Ditsworth et al., 2017). Evidence from ALS patients and *SOD1* mouse models also shows
9 early loss of neuromuscular junctions (NMJ) prior to disease onset (Fischer et al., 2004; Pun et
10 al., 2006; Hegedus et al., 2007; Hegedus et al., 2008; Martineau et al., 2018), supporting the
11 notion that ALS has a long silent pre-symptomatic phase (Eisen et al., 2014). Interestingly, an
12 early and persistent functional alteration of perisynaptic Schwann cells (PSCs), glial cells at the
13 NMJ, was reported in the *SOD1*^{G37R} mouse model (Arbour et al., 2015).

14 Early PSC dysfunction in ALS could be of particular importance owing to their ability to
15 detect and modulate synaptic communication, regulate NMJ stability and oversee NMJ repair.
16 Importantly, these three functions are interdependent as PSC synaptic decoding regulates their
17 ability to stabilize or repair NMJs, notably through muscarinic receptors (mAChRs). Indeed,
18 activation of PSC mAChRs and purinergic receptors triggers a transient increase in cytoplasmic
19 calcium (Ca²⁺ response), through which they modulate neurotransmitter release (Robitaille,
20 1998; Rochon et al., 2001; Rousse et al., 2010; Todd et al., 2010). Blockade of PSC mAChRs
21 destabilizes NMJs (Wright et al., 2009), demonstrating that proper PSC synaptic decoding is
22 necessary for NMJ maintenance.

1 Importantly, PSCs contribute to NMJ re-innervation following denervation of NMJs by
2 adopting a “pro-regenerative” (repair) phenotype. For instance, PSCs extend long processes
3 known to guide re-innervation through nerve terminal sprouting (Reynolds and Woolf, 1992;
4 Son and Thompson, 1995b, a; Son et al., 1996; O'Malley et al., 1999). Similarly to axonal
5 Schwann cells (SCs) (Reichert et al., 1994; Painter et al., 2014; Brosius Lutz et al., 2017), PSCs
6 also actively phagocytose presynaptic debris following denervation (Duregotti et al., 2015)
7 which is essential for efficient axonal regrowth and NMJ re-innervation (Kang and Lichtman,
8 2013). Finally, complete PSC endplate coverage is essential for re-innervation since parts of the
9 endplate vacated by PSCs are forsaken during re-innervation (Kang et al., 2014). Importantly,
10 mAChRs activation represses PSC’s repair phenotype and can modulate NMJ repair by
11 regulating PSC gene expression (Georgiou et al., 1994; Georgiou et al., 1999).

12 Interestingly, Arbour et al. (2015) reported an enhanced mAChR contribution to PSC
13 Ca²⁺ responses at NMJs innervated by disease-resistant or moderately vulnerable MUs (S and FR
14 MU respectively, *Soleus* (SOL) muscle) in *SOD1*^{G37R} mice. As previously proposed (Ko and
15 Robitaille, 2015; Arbour et al., 2017), we postulated that inappropriate mAChR signaling could
16 prevent PSCs from adopting a repair phenotype, thus hindering NMJ reinnervation in ALS.
17 However, this repair phenotype remains unevaluated in symptomatic animals. Furthermore,
18 recent evidence revealed opposite changes in the synaptic properties of NMJs from different MU
19 types in *SOD1*^{G37R} mice (Tremblay et al., 2017). This raises the possibility that PSC properties,
20 notably mAChR overactivation, may be different at NMJs innervated by vulnerable FF MUs.

21 In the present study, we assessed if PSCs mAChR overactivation was also present at
22 NMJs innervated by vulnerable FF MUs in the *Sternomastoid* (STM) muscle at different stages
23 of the disease. Next, we evaluated if PSCs adopted a repair phenotype, either in presymptomatic

1 SOD1^{G37R} animals following experimentally-induced denervation, or in symptomatic SOD1^{G37R}
2 mice where the progressive denervation of NMJs is ongoing. Notably, we evaluated the presence
3 of extended processes, nerve terminal sprouts and phagocytic markers at vulnerable (STM or
4 EDL) or partially resistant (SOL) NMJs. Albeit through a different mechanism, PSCs in the STM
5 also displayed an early, but transient, increase in mAChR-dependent decoding. Consistent with
6 defects in PSC-dependent NMJ repair mechanisms in all these muscles, PSCs displayed
7 abnormal process extension as well as paradoxical expression of Galectin-3 (MAC-2), a marker
8 of glial phagocytosis. Altogether, these results suggest that changes in PSCs are maladapted in
9 ALS.

10

1 MATERIALS AND METHODS

2 *Animals*

3 Male transgenic mice heterozygote for the human *Sod1* gene carrying the *G37R* mutation
4 (*SOD1^{G37R}*, line 29; [B6.Cg-Tg(SOD1*G37R)29Dpr/J]; stock number 008229), or, in some
5 experiments, the *G93A* mutation (*SOD1^{G93A}*; [B6SJL-Tg(SOD1*G93A)1Gur/J]; stock number
6 002726), were obtained from The Jackson laboratories (Bar Harbor, ME). *SOD1^{G37R}* mice were
7 maintained on a C57BL/6 background and were genotyped by PCR for the *hSOD1* gene
8 performed on a tail sample taken at the time of the weaning.

9 For some experiments, transgenic mice expressing the “yellow fluorescent protein”
10 (YFP) in all motor neurons (Feng et al., 2000) were used (homozygous *Thy1-YFP*, line 16;
11 [B6.Cg-Tg(Thy1-YFP)16Jrs/J]; stock number 003709). These mice were also obtained from The
12 Jackson laboratories (Bar Harbor, ME) and were maintained on a C57BL/6 background.

13 Pre-symptomatic *SOD1^{G37R}* mice were used at P119-131 (P120) and P179-194 (P180)
14 (Figure 1A). Phenotypically matched late symptomatic *SOD1^{G37R}* mice were used between P505
15 and P565. Age-matched *wild-type* (*WT*) brothers were used as controls. Animals were sacrificed
16 by exposition to a lethal dose of isoflurane (CDMV, Saint-Hyacinthe, Qc, Canada, J2S 7C2). All
17 experiments were performed in accordance with the guidelines of the Canadian Council of
18 Animal Care and the Comité de déontologie animale of Université de Montréal.

19

20 *Phenotype evaluation*

21 Starting at P290 or earlier, mice were weighted weekly to assess disease onset and
22 progression as previously described (Lobsiger et al., 2009; Parone et al., 2013). Briefly, disease
23 onset and early disease were defined as peak body weight and 10% loss from peak body weight

1 respectively. Consistent with the recent reduction in transgene copy number in this line
2 (Zwiegers et al., 2014), the median age of onset of the symptomatic animals used in this study
3 was 456 days, while the median age of early disease was 506 days (Fig. 1A; N=19).
4 Phenotypically matched symptomatic animals were sacrificed for experimentation when 3
5 criteria were met (P505-P565) and are hereafter referred to as “symptomatic *SOD1*^{G37R} mice”:
6 (1) they passed the early disease stage (10% weight loss); (2) they displayed hindlimb paralysis
7 as assessed by tail suspension; and (3) they showed a reduced grid hanging time (less than 10
8 seconds). The average duration of the disease progression (from age of onset to sacrifice) was
9 78.26 ± 6.40 days.

10

11 ***Sciatic nerve crush surgery***

12 Mice were anesthetized using isoflurane (2-3% in 98-97% O₂) in an induction chamber
13 and anesthesia was then maintained under a breathing mask. Lubricant (Optixcare) was applied
14 on the eyes to prevent dryness. Mice were placed in prone position and an incision was made on
15 the left mid-thigh. The *gluteus maximus* and the *biceps femoris muscles* were delicately separated
16 to expose the sciatic nerve. The nerve was then crushed with Moria microserrated curved forceps
17 (MC31; maximal pressure for 15s). Muscles were then gently repositioned and the wound closed
18 using 5-0 or 6-0 Vicryl suture (CDMV). Buprenorphine (3µg/10g of body weight; Temgesic)
19 was subcutaneously administered three times during the following 24 hours. At the end of the
20 surgery, mice were also injected subcutaneously with 0.25 mL of warm 0.9% saline twice to
21 prevent dehydration. For sham-operated animals, the same procedure was followed, but the
22 sciatic nerve was only exposed and not crushed.

23

1 *Sternomastoid calcium imaging*

2 Both *STM* muscles and their nerves were dissected from the same animal in oxygenated
3 Ringer REES solution containing (in mM): 110 NaCl, 5 KCl, 25 NaHCO₃, 2 CaCl₂, 1 MgCl₂, 11
4 Glucose, 0.3 Glutamic Acid, 0.4 Glutamine, 5 BES (N,N-Bis(2-hydroxyethyl)taurine), 0.036
5 Choline Chloride, 4.34 x 10⁻⁴ Thiamine pyrophosphate (all Sigma-Aldrich). Muscles were
6 pinned in a Sylgard184-coated (Dow Corning) recording chamber and the nerves were placed in
7 two suction electrodes and were independently stimulated using a Pulsemaster A300 stimulator
8 (square pulses: 20mV to 2V, 0.1ms duration; WPI). PSCs were loaded with the fluorescent Ca²⁺
9 indicator Rhod-3 (Life Technologies) by incubating muscles twice for 45 min in preoxygenated
10 Ringer containing 5 μM Rhod-3 AM (Life Technologies), 0.02 % Pluronic acid (Life
11 Technologies) and 0.15% dimethyl sulfoxide (DMSO) at 29 ± 2°C (Todd et al., 2010; Arbour et
12 al., 2015). NMJs were located by labelling nAChRs prior to the start of the experiment with a
13 closed-bath application of Alexa 488-conjugated α-BTX (5 μg for 10 min; Life Technologies).
14 PSCs were easily identified using transmitted light microscopy and their identity was further
15 confirmed through their apposition over BTX staining. . For experiments performed at P180,
16 changes in fluorescence were monitored using a Zeiss LSM510 confocal microscope equipped
17 with a 40x water-immersion lens (NA: 0.8; Zeiss). Rhod-3 was excited using a 543nm HeNe
18 laser and emission was filtered using a 560nm long-pass filter. For experiments performed on
19 symptomatic animals, changes in fluorescence were monitored using an Olympus FV-1000
20 confocal microscope equipped with a 60x water-immersion lens (NA: 0.9; Olympus). Rhod-3
21 was excited using a 559 nm diode laser and emission detected through a 570-625 nm spectral
22 window. Changes in fluorescence were measured on the PSCs soma using the ImageJ software
23 and were expressed as % $\Delta F/F_0 = (F - F_0)/F_0$. Recordings of PSC Ca²⁺-responses were not

1 included when baseline fluorescence was unstable, focus changes occurred, spontaneous Ca^{2+}
2 activity was observed or when Ca^{2+} levels did not return to the baseline after PSC activation. No
3 direct comparisons between data obtained on different systems were made.

4 Ca^{2+} responses to endogenous neurotransmitter release were evoked by high-frequency
5 stimulation of the nerve (50Hz, 20s). This pattern is known to elicit robust neurotransmitter
6 release in this preparation (Wyatt and Balice-Gordon, 2008) and to efficiently trigger PSC Ca^{2+}
7 responses in another fast-twitch muscle (Rousse et al., 2010). Alternatively, PSC mAChRs or
8 purinergic receptors were activated by local application of agonists diluted in the extracellular
9 Ringer REES solution, respectively muscarine (10 μM ; Sigma) or ATP (1 μM ; Sigma). Local
10 drug application was achieved by applying a brief pulse of positive pressure (20 PSI, 150ms)
11 using a Picospritzer II (Parker Instruments) through a glass micropipette ($\sim 2 \mu\text{m}$ tip, $5\text{M}\Omega$)
12 positioned next to the NMJ. Because of the rundown of PSC Ca^{2+} responses following repeated
13 activation (Jahromi et al., 1992; Rochon et al., 2001), local applications of agonists were
14 performed before the high-frequency nerve stimulation was performed, each agonist was applied
15 only once on each NMJ, and ATP and muscarine were applied at least 20 minutes apart on any
16 given NMJ . Only a single high-frequency stimulation was executed on each muscle and PSC
17 Ca^{2+} -responses were imaged on a naïve NMJ. NMJs where high frequency nerve stimulation did
18 not induce a presynaptic Ca^{2+} increase were discarded.

19 In all experiments, muscles were perfused (60-80 mL/h) with heated ($28 \pm 1 \text{ }^\circ\text{C}$) Ringer
20 REES containing 2.3 $\mu\text{g}/\text{mL}$ of D-tubocurarine (Sigma) to prevent muscle contraction during
21 nerve stimulation. In some experiments, mAChRs were blocked by adding the non-selective
22 antagonist Atropine (10 μM ; Sigma) to the extracellular Ringer REES solution. To ensure
23 efficient blocking of mAChRs, muscles were perfused at least 45 min prior to the start of the

1 experiment. PSCs responding to local application of muscarine after Atropine blockade were
2 discarded.

3

4 ***Whole-mount muscle preparations and immunohistochemistry***

5 The *Sternomastoid* (STM) muscle is divided in two easily distinguishable parts on its
6 ventral side: a lateral part composed exclusively of fast-fatigable (FF) motor-units (MUs) on the
7 surface (the “white” part), and a medial part composed of a mixture of FF and fast-fatigue-
8 resistant (FR) MUs (the “red” part) as inferred by their fiber type composition (Fig.1B et C)
9 (Brichta et al., 1987). To exclusively evaluate vulnerable FF MUs in all experiments, we
10 restricted our analysis to the “white” part of the STM which is easily observable using
11 transmitted light. All surface NMJs analyzed in the *Extensor digitorum longus* (EDL) were
12 associated with vulnerable FF MUs as previously shown (Tremblay et al., 2017). All NMJs
13 analyzed in the *Soleus* (SOL) were associated with either fast-fatigue-resistant (FR) or slow (S)
14 motor-units (MUs) as previously described (Pun et al., 2006; Arbour et al., 2015; Tremblay et
15 al., 2017).

16 Immunohistochemical labeling was performed as described elsewhere (Todd et al., 2010;
17 Darabid et al., 2013; Arbour et al., 2015). STM and SOL muscles were dissected in oxygenated
18 (95% O₂, 5% CO₂) REES physiological solution and were pinned in a Sylgard-coated (Dow
19 Corning) 10 mm petri dish and fixed for 10 min in 4% formaldehyde (Mecalab) diluted in PBS
20 (in mM: 137 NaCl, 10 Na₂HPO₄, 2.7 KCl, 2 KH₂PO₄; all Sigma-Aldrich) at room temperature
21 (RT). Then, muscles were permeabilized in 100% ice-cold methanol for 6 min at -20°C and non-
22 specific labeling was reduced using 10 % normal donkey serum (NDS) diluted in PBS containing
23 0.01% Triton X-100 (20 min incubation). Muscles were incubated overnight at 4°C with a rat

1 IgG2a anti-MAC-2 (Galectin-3) antibody (1:250; clone M3/38; Cedarlane, cat# CL8942AP),
2 then 2h at RT with a rabbit IgG anti-S100 β antibody (1:250; Dako-Agilent, cat# Z031101-2 or
3 between 1:4 and 1:5, Dako-Agilent, cat#IR50461-2) followed by 2h at RT with the chicken IgY
4 anti- Neurofilament medium chain (NF-M; 1:2000; Rockland Immunochemicals; cat# 212-901-
5 D84) and the mouse IgG1 anti-synaptic vesicular protein 2 (SV2; 1:2000; Developmental Studies
6 Hybridoma bank; concentrate) antibodies. Secondary antibodies donkey anti-rabbit IgG Alexa-
7 594, donkey anti-rat IgG Alexa-647, goat anti-mouse IgG1 Alexa-488 and donkey anti-chicken
8 Alexa-488 were incubated together for 1h at RT (all 1:500; Jackson ImmunoResearch). All
9 antibody dilutions were made in PBS buffer containing 0.01% Triton X-100 and 2% NDS.
10 Finally, postsynaptic nicotinic receptors (nAChRs) were labeled using α -Bungarotoxin (BTX)
11 conjugated with CF405 (4 μ g/mL; Biotium; cat ##00002) for 45 min in PBS. In some cases
12 (nerve crush experiment at P90, Fig.7A), the anti-SV2 antibody was replaced with goat anti-
13 synaptotagmin (SyT; 1:250). In these cases goat anti-mouse IgG1 Alexa-405, donkey anti-
14 chicken Alexa-405 (both 1:250; Jackson ImmunoResearch), donkey anti-rabbit IgG Alexa 488
15 (1:500; Jackson ImmunoResearch) and α -BTX conjugated to Alexa-594 (1.33 μ g/mL; Life
16 Technologies; cat# B13423) were used instead. After each incubation (except NDS blocking),
17 muscles were rinsed three times for 5 min in PBS containing 0.01% Triton X-100. Muscles were
18 mounted in ProlongGold anti-fade reagent (Life Technologies). Images were acquired on an
19 Olympus FV1000 confocal microscope equipped with a 60x oil-immersion objective (N.A: 1.4;
20 Olympus). Fluorescence was excited using a 488 nm (Alexa-488) argon laser and a 405 nm, a
21 559 nm and a 633 nm laser diode. Fluorescence emission was filtered using appropriate custom
22 spectral windows (425 – 475nm, 500 – 545 nm, 570 – 630nm and 650 – 750nm). For figure

1 representation, gamma was adjusted to enhance visibility of certain NMJ structures using Adobe
2 Photoshop. No quantitative measurements were performed on the adjusted images.

3 For some experiments, muscles were fixed and immunolabeled after calcium imaging
4 experiments to determine their innervations status post-hoc. In these experiments, confocal
5 stacks of the BTX labeling pattern of the imaged and neighboring NMJs were acquired live and
6 were used to re-identify the same NMJs following immunolabeling as previously described
7 (Arbour et al., 2015).

8

9 ***Gal-3 labeling on non-permeabilized whole-mount muscle tissue***

10 To label extracellular *Gal-3*, muscles from Thy1-YFP animals were fixed in 4%
11 formaldehyde and non-specific labeling was blocked using 10% NDS. Muscles were then
12 incubated overnight at 4°C with the rat IgG2a anti-MAC-2 (Galectin-3) antibody (1:100), which
13 was then revealed using a donkey anti-rat IgG Alexa-647 antibody (1:500; 60 min). Postsynaptic
14 nAChRs were labeled with BTX conjugated to Alexa-594 (5µg/mL; 45 min). Muscles were
15 rinsed three times for 5 min each between incubations and all dilutions and rinses were made in
16 PBS buffer without Triton X-100. Muscles were then mounted in Prolong Diamond anti-fade
17 reagent containing DAPI (Life technologies). Using this approach, no labeling of the presynaptic
18 markers SV2 and NF-M could be observed, confirming that cells were not inadvertently
19 permeabilized during the procedure (*data not shown*).

20

21 ***Analysis of NMJ morphology***

22 Analysis of NMJ morphology was performed using the seven criteria previously
23 described and illustrated by Tremblay et al. (2017). Briefly, NMJ innervation and postsynaptic

1 receptor organization (faint clustered or ectopic nAChRs) were analyzed and the presence of
2 nerve terminal sprouting, polyinnervation and PSC process extensions was quantified. Although
3 PSCs downregulate the S100 β marker following denervation (Magill et al 2007), PSC somata on
4 fully denervated endplates were still discernible, allowing quantification of Galectin-3
5 expressing PSCs. NMJs without any detectable S100 β staining (presumably denervated for a
6 long time) were not included in this study. Notwithstanding the limitations of S100 β for the
7 quantification of PSC process extensions in these conditions (Son and Thompson, 1995a), a large
8 number of processes were labeled allowing quantification based on their presence on an NMJ
9 rather than their number. Furthermore, we never observed a Galectin-3-positive S100 β -negative
10 process or a presynaptic sprout in absence of S100 β staining, showing that S100 β is reliable for
11 this analysis in these conditions.

12

13 ***Muscle cross-section immunohistochemistry***

14 Immunostaining was performed similarly as previously described (Tremblay et al.,
15 2017). Briefly, the *STM* muscle was dissected and frozen in cold optimal cutting medium
16 compound (OCT; TissueTek) using isopentane at -80°C. Transverse cryosections (10 μ m) were
17 made and incubated in blocking solution (10% NDS in PBS). Sections were incubated with
18 either mouse IgG1 anti-MHC type IIa (SC-71, 1:200), mouse IgG2b anti-MHC type I (BA-D5,
19 1:100) and mouse IgM anti-MHC type IIb (BF-F3, 1:200) or mouse IgM anti-MHC type IIx
20 (6H1; 1:10) and mouse IgG1 anti-MHC all but IIx (BF-35, 1:200) for 1h at room temperature (all
21 from Developmental Studies Hybridoma bank; concentrates (Schiaffino et al., 1989; Lucas et al.,
22 2000)). They were revealed with appropriate secondary antibodies (1:500, Jackson
23 Immunoresearch) and mounted in Prolong Gold antifade reagent (Life Technologies).

1

2 ***Experimental design and statistical analyses***

3 For Ca²⁺ imaging experiments, the number of animals used (N; biological replicates) and
4 the number of PSCs analyzed (n; statistical replicates) are indicated in the text. Unpaired *t*-tests
5 were performed to compare two different conditions from different experiments. *Two-way*
6 *ANOVAs* tests were used to evaluate the effect of two independent variables on Ca²⁺-responses,
7 using *Tukey's multiple comparisons (Tukey's test)* as a *post-test*. To analyze the heterogeneity of
8 Ca²⁺ responses belonging to the same NMJs, the amplitude of the response of each cell was
9 expressed as a percentage of the average response of all imaged cells on that NMJ. Then, the
10 standard deviation of the resulting distribution for each group were compared using the *F test for*
11 *unequal variance*, using *Holm-Sidak's* method to correct for multiple comparisons. Statistical
12 tests were performed in GraphPad Prism 7 software. Unless otherwise stated, all results are
13 presented as mean ± SEM. All tests used a confidence interval of 95% ($\alpha = 0.05$).

14 For the morphological analysis, all visible surface NMJs from left and right STM and
15 SOL muscles were included. Number of animals used (N; representing both the biological and
16 statistical replicates) and the number of NMJs or PSCs analyzed (n; number of observations) in
17 each condition are indicated in the text. Due to the nature of the analysis (count data), the data
18 does not meet the assumptions of following a Gaussian Distribution or having a variance equal
19 between groups and symmetric (Crawley, 2007). Hence, *Generalized linear models (GLM)* were
20 created, using a binomial error structure and a logit link function (logistic distribution), to
21 analyze the results as previously described (Tremblay et al., 2017). For all criteria, the effect of
22 the genotype (WT vs SOD1^{G37R}) and the muscle (STM vs SOL) were evaluated. Furthermore,
23 the effect of the innervation status of NMJs (fully innervated vs completely denervated) on

1 PSCs' repair response, identified by process extensions and Gal-3 expression, was also
2 evaluated. The muscle and the innervation status were defined as within-subject factors. The
3 effects of all 2-way and 3-way interactions were also evaluated. Finally, biologically relevant
4 pairwise comparisons are illustrated in Figure 5A and were made using the estimated marginal
5 means (EM means), using *Holm-Sidak's* method to correct for multiple comparisons (hereafter
6 referenced by *GLM post-test*). All analyses were made using the SPSS software (v.24.0.0.0;
7 IBM). All tests used a confidence interval of 95% ($\alpha = 0.05$).

1 RESULTS

2 We have previously shown an increased activation of PSC mAChR during synaptic
3 communication at S and FR NMJs in presymptomatic *SOD1^{G37R}* mice (P120 and P380) (Arbour
4 et al., 2015). However, NMJs innervated by different MU-types display opposite changes in their
5 synaptic properties in *SOD1^{G37R}* mice, i.e. neurotransmitter release is increased at S NMJs and
6 decreased at FF NMJs (Tremblay et al., 2017). Knowing that alterations in synaptic activity can
7 induce plastic changes in PSC activity (Belair et al., 2010), PSC excitability may be different at
8 FF NMJs in *SOD1^{G37R}* mice. In the present study, we first tested whether PSCs at vulnerable FF
9 NMJs also displayed an enhance mAChR activation during synaptic communication (mAChR
10 contribution) in *SOD1^{G37R}* mice. For most experiments, the STM, (FF MUs on its ventro-lateral
11 face; Fig. 1B and 1C), and the SOL (FR and S MUs; Arbour et al., 2015) nerve muscle
12 preparations were used due to their similar rate of denervation in *SOD1* mice despite their
13 different MU type composition (Valdez et al., 2012). Their similar disease course allowed the
14 analysis of the impact of the MU type on PSC repair properties under similar levels of
15 endogenous denervation (symptomatic animals). FF NMJs in the STM of *SOD1^{G37R}* mice also
16 showed a similar decrease in synaptic activity (*unpublished observations*) to FF NMJs in the
17 EDL at P180 (Tremblay et al., 2017), indicating that, despite denervation occurring at later
18 stages than in hindlimb fast-twitch muscles, early synaptic alterations are also present in the
19 STM.

20

21 ***Reduced PSC Ca²⁺ activity in the STM of presymptomatic *SOD1^{G37R}* mice***

22 First, we examined the ability of PSCs to detect endogenous neurotransmitter release
23 elicited by a motor nerve stimulation (50 Hz 20 sec) in the STM. PSC activity was monitored by

1 imaging transient intracellular Ca^{2+} changes, a well-established reporter of their decoding
2 activity (Rochon et al., 2001; Rousse et al., 2010). Experiments were performed at P120, age
3 where the first alterations were observed in the SOL of *SODI*^{G37R} mice (Arbour et al., 2015). At
4 this stage, no signs of denervation were observed in the STM of *SODI*^{G37R} mice (Fig. 1D; 50
5 NMJs, N=2).

6 At P120, all PSCs of *WT* (18 PSCs; 9 NMJs; N=6) and *SODI*^{G37R} mice (19 PSCs; 7
7 NMJs; N=4) responded to nerve stimulation-induced neurotransmitter release in the STM. PSC
8 Ca^{2+} response amplitude was similar between *WT* and *SODI*^{G37R} mice (333.7 ± 31.1 % $\Delta\text{F}/\text{F}_0$,
9 $n=18$ vs 279.2 ± 27.4 % $\Delta\text{F}/\text{F}_0$, $n=19$ respectively; $t_{(35)}=1.320$; $p=0.1954$ *Unpaired t-test*). This is
10 consistent with the different progression of limb and trunk muscles and the observation that PSC
11 Ca^{2+} responses were unchanged in the SOL 2 months earlier (P60) (Arbour et al., 2015).

12 We next examined PSC properties in the STM at P180 to test whether changes in PSC
13 activity were delayed in the STM compared to the SOL. Again, PSCs responsiveness to nerve
14 stimulation was similar between *SODI*^{G37R} and *WT* mice (*SODI*^{G37R}: 31 out of 33 PSCs; 12
15 NMJs; N=8; *WT*: 20 out 22 PSCs; 11 NMJs; N=8). However, unlike at P120, PSC Ca^{2+}
16 responses at P180 were significantly smaller in *SODI*^{G37R} mice (Fig 2A and 2D; *WT-Ctrl* : 403.2
17 ± 22.8 % $\Delta\text{F}/\text{F}_0$, $n=20$ vs *SODI-Ctrl*: 270.6 ± 24.3 % $\Delta\text{F}/\text{F}_0$, $n=31$; Effect of genotype:
18 $F_{(1,77)}=25.13$; $p<0.0001$, *Two-way ANOVA*; $p=0.0005$, *Tukey's test on Two-way ANOVA*). Hence,
19 PSC properties were also altered in the STM of *SODI*^{G37R} mice at an early presymptomatic
20 stage, but in an opposite manner to what was observed in the SOL (Arbour et al., 2015).

21

22

23

1 ***Relative increase of mAChR-dependent PSC activity in STM at a presymptomatic stage***

2 Next, we tested whether the contribution of mAChR activation to PSC Ca²⁺ activity
3 (mAChR contribution) was increased in the STM, despite the smaller PSC Ca²⁺ responses.

4 For this, Ca²⁺ imaging was performed in presence of the general mAChR antagonist
5 Atropine (10 μM) at P180. As shown in Figure 2B, blockade of PSC mAChRs was confirmed
6 before the nerve stimulation by the inability of local muscarine applications (10 μM) to elicit
7 Ca²⁺ responses. Out of the 32 cells analyzed (14 in *WTs* and 18 in *SOD1s*), only 2 PSCs from *WT*
8 mice exhibited a small response to local application of muscarine in presence of atropine and
9 were discarded. In the presence of atropine, all PSCs responded to nerve stimulation-induced
10 neurotransmitter release in both *WT* (12 PSCs; 7 NMJs; N=4) and *SOD1*^{G37R} mice (18 PSCs; 8
11 NMJs; N=4). As expected, the amplitude of PSC Ca²⁺ responses was significantly decreased in
12 both groups (Effect of atropine: $F_{(1,77)}=22.63$ $p<0.0001$; *Two-way ANOVA*; Interaction:
13 $F_{(1,77)}=0.01446$, $p=0.9046$). In *WT* mice, it was reduced from 403.2 ± 22.8 % $\Delta F/F_0$, (n=20) to
14 277.5 ± 18.4 % $\Delta F/F_0$ in presence of atropine (n=12; $p=0.0194$; *Tukey's test on Two-way*
15 *ANOVA*). This represents a 31% contribution of mAChRs to PSC Ca²⁺ responses that is similar
16 to our observation in the adult SOL (Arbour et al., 2015). Likewise, PSC Ca²⁺ responses in
17 *SOD1*^{G37R} mice had a significantly smaller amplitude in presence of atropine (Fig. 2D; *SOD1*-
18 Ctrl: 270.6 ± 24.3 % $\Delta F/F_0$, n=31 vs *SOD1*-Atropine: 138.5 ± 27.6 % $\Delta F/F_0$, n=18; $p=0.0013$;
19 *Tukey's test on Two-way ANOVA*). However, this represents a 49% mAChR contribution in
20 *SOD1*^{G37R} mice, which is 1.6-fold larger than in *WT* animals. Hence, the contribution of mAChR
21 activation to PSC Ca²⁺-activity is also increased in the STM of *SOD1*^{G37R} mice.

22 Furthermore, PSC Ca²⁺ responses in *SOD1*^{G37R} mice remained significantly smaller than
23 in *WT* mice in presence of atropine ($p=0.0094$; *Tukey's test on Two-way ANOVA*). As such, the

1 reduction of the amplitude of PSC Ca^{2+} responses in the STM of *SODI*^{G37R} seem to be
2 attributable to the reduced activation of non-muscarinic PSC receptors. The other major type of
3 receptors by which PSCs detect synaptic activity at the mammalian NMJ are purinergic receptors
4 (Rochon et al., 2001). However, their specific contribution to nerve-evoked PSC Ca^{2+} -response
5 was not evaluated as the underlying set of receptors remain undetermined at the adult
6 mammalian NMJs (Rochon et al., 2001; Arbour et al., 2015).

7 As a whole, these results suggest that a relative increase in the contribution of mAChR to
8 PSC activity is a common pathological feature between both fast-twitch and slow-twitch muscles
9 in *SODI*^{G37R} mice.

10

11 ***Heterogeneous nerve-induced PSC activity at individual NMJs in the STM at a*** 12 ***presymptomatic stage***

13 Interestingly, PSCs belonging to the same NMJ in the STM of *SODI*^{G37R} mice displayed
14 heterogeneous responses to nerve stimulation, an unseen characteristic in *WT* mice (Fig. 3A).
15 When only considering NMJs where multiple PSCs were imaged, PSC Ca^{2+} responses were all
16 within $\pm 20\%$ of the average response on their NMJ in *WT* animals (Fig. 3B; SD = 11.17 %;
17 N=8; n=20). However, in *SODI*^{G37R} mice, PSC Ca^{2+} responses ranged from -99 % up to +85 %
18 of the average response on their NMJ (Fig. 3B; SD = 43.65 %; N=8; n=31), which is
19 significantly more than in *WT* mice ($F_{(30,19)}=15.27$; $p=0.0004$; *F-test*). This suggests an uneven
20 alteration of PSCs excitability at presymptomatic stage.

21 These results could imply that the increased mAChR-dependent PSC activity is also
22 uneven in the STM of *SODI*^{G37R} mice and therefore may not be a common feature to all PSCs. If
23 this were the case, blockade of PSC mAChRs would restore homogeneity in Ca^{2+} responses over

1 a single NMJ. However, heterogeneity in PSC Ca^{2+} responses was maintained following
2 blockade of mAChRs in *SOD1^{G37R}* mice (Fig. 3C). In presence of atropine, PSC Ca^{2+} responses
3 in *WT* animals varied between -20 % to +30 % of each other on a given NMJ (Fig. 3D; N=4;
4 n=9; SD=15.12 %;) while PSC Ca^{2+} responses in *SOD1^{G37R}* mice varied between -71 % and +113
5 % (Fig. 3D; N=3; n=15; SD=47.51 %), thus maintaining the difference observed in control
6 condition ($F_{(14,8)}=9.877$; $p=0.0087$; *F-test*). Indeed, presence of atropine did not significantly
7 affect the variability of Ca^{2+} -responses on single NMJs in *WT* (*WT-Ctrl* vs *WT-Atropine*:
8 $F_{(8,19)}=1.832$; $p=0.4610$; *F-test*) or in *SOD1^{G37R}* mice (*SOD1-Ctrl* vs *SOD1-Atropine*:
9 $F_{(14,30)}=1.185$; $p=0.6702$; *F-test*). These results reveal that heterogeneity in PSC Ca^{2+} responses in
10 *SOD1^{G37R}* mice is independent of mAChR activation. Hence, increased relative mAChR
11 contribution to PSC synaptic decoding appears to be present in all PSCs in the STM of *SOD1^{G37R}*
12 mice.

13

14 ***Reduced PSC detection of purinergic signals in STM of presymptomatic SOD1^{G37R} mice***

15 PSC Ca^{2+} activity heavily depends on their intrinsic properties (Belair et al., 2010;
16 Rousse et al., 2010; Darabid et al., 2013; Arbour et al., 2015), such as the presence and
17 sensitivity of their muscarinic and purinergic receptors. To further investigate PSC properties in
18 the STM of *SOD1^{G37R}* mice, we first tested PSCs sensitivity to cholinergic signals by monitoring
19 PSC Ca^{2+} responses elicited by local application of the mAChR agonist muscarine (10 μM). As
20 shown in Figure 4A, PSCs in both groups exhibited similar responsiveness (*WT*: 28 out 32; 17
21 NMJs; N=10 vs *SOD1*: 32 out of 33; 16 NMJs; N=8) and Ca^{2+} responses of similar amplitude
22 following muscarine application (Fig. 4B; 191.6 ± 23.1 % $\Delta\text{F}/\text{F}_0$, n=28 vs 228.0 ± 23.0 % $\Delta\text{F}/\text{F}_0$
23 , n=32, respectively; $t_{(58)}=1.127$; $p=0.2644$; *Unpaired t-test*). Thus, these results are consistent

1 with the suggested reduced activation of another type of PSC receptors during synaptic
2 communication in the STM of *SOD1^{G37R}* mice.

3 Next, PSCs' sensitivity to purinergic agonists was examined by monitoring PSC Ca²⁺
4 responses after local application of the general purinergic agonist ATP (1μM). Local application
5 of ATP robustly triggered a Ca²⁺ response in 100% of PSC in both groups (*WT*: 32 out of 32; 15
6 NMJs; N=9 vs *SOD1*: 21 out 21; 13 NMJs; N=7). However, as shown in Figure 4C, ATP-
7 induced PSC Ca²⁺ responses in the STM of *SOD1^{G37R}* mice were smaller than in *WT* mice (Fig.
8 4D; 315.2 ± 35.6 % $\Delta F/F_0$, n=21 vs 394.3 ± 20.2 % $\Delta F/F_0$, n=32, respectively; $t_{(51)}=2.078$;
9 $p=0.0429$; *Unpaired t-test*). These results suggest that PSCs are less sensitive to purinergic
10 signals in the STM of *SOD1^{G37R}* mice.

11 Altogether, our results obtained by imaging PSC Ca²⁺ activity show that the relative
12 contribution of mAChR to PSC activity is increased, while PSCs' sensitivity to purinergic
13 signals is decreased at FF NMJs in *SOD1^{G37R}* mice. Despite having slightly different properties
14 depending on the MU type they are associated with (Arbour et al., 2015), these results show that
15 the contribution of mAChR to PSCs' activity increases at all NMJ types in *SOD1^{G37R}* mice.

16

17 ***PSCs express and secrete the phagocytic marker Gal-3 following denervation in WT mice***

18 Knowing that PSC mAChR activation regulates gene expression and represses their
19 repair phenotype, we postulated that altered muscarinic properties would be associated with
20 defects in PSC-dependent NMJ repair mechanisms. Notably, PSCs become phagocytic and
21 participate in the clearance of nerve terminal debris following denervation (Duregotti et al.,
22 2015) similarly to axonal SCs (Reichert et al., 1994; Brosius Lutz et al., 2017). Axonal debris

1 clearance is essential for efficient NMJ reinnervation, cellular debris hindering axonal growth in
2 the endoneural tube (Kang and Lichtman, 2013).

3 Interestingly, phagocytic axonal SCs express the β -galactoside-binding lectin Galectine-3
4 (Gal-3, a.k.a MAC-2) (Reichert et al., 1994; Rotshenker et al., 2008), similarly to other
5 phagocytic glial cells (Rotshenker, 2009; Nguyen et al., 2011; Morizawa et al., 2017), suggesting
6 that its expression could also reflect PSC phagocytic activity. However, Gal-3 expression has
7 never been evaluated in PSCs. Thus, we first investigated whether PSCs expressed Gal-3 at
8 denervated NMJs in *WT* animals by performing an IHC for the three synaptic components
9 (presynaptic, postsynaptic and glia) and Gal-3. We induced the complete denervation of SOL
10 NMJs in adult *WT* animals by sciatic nerve crush and monitored the presence of Gal-3 two days
11 later (Fig. 5A; Nerve crush: N=3, n=43; Sham: N=3, n=42). As expected, we observed a robust
12 expression of Gal-3 in the soma and processes of PSCs following sciatic nerve crush (Fig. 5A, E;
13 85.66 ± 2.02 % of PSCs, n=134) compared to sham surgery (2.883 ± 1.92 % of PSCs, n=105;
14 $p < 0.001$; *GLM post-test*). These results confirm that PSCs express Gal-3 following NMJ
15 denervation as part of their normal response to injury in *WT* animals.

16 Gal-3 can be present intracellularly, secreted or associated with transmembrane proteins
17 (Dumic et al., 2006; Yang et al., 2008). Previous studies on axonal SCs suggested that Gal-3 may
18 exert its function in the extracellular space (Reichert et al., 1994). To further characterize its role
19 at the NMJ, we examined whether Gal-3 was present in the extracellular space two days after
20 sciatic nerve crush by performing an IHC in absence of membrane permeabilization. Since our
21 presynaptic markers are intracellular, the efficacy of the denervation was validated by
22 performing experiments on animals expressing the “yellow fluorescent protein” (YFP) in all
23 motor neurons (homozygous Thy1-YFP16 mice). As shown in Figure 5B, Gal-3 was present in

1 the extracellular space following sciatic nerve crush (Fig. 5B₁; N=3, n=45) but not sham surgery
2 (Fig. 5B₂; N=2, n=27). Extracellular Gal-3 seemed membrane bound as it was present all around
3 PSCs' somata (Fig. 5B₃). However, close comparison of Gal-3 staining in permeabilized and
4 non-permeabilized tissue (Fig 5A₃ and 5B₃ respectively) reveals that part of the staining was
5 missing in non-permeabilized tissues (asterisk). This difference shows that Gal-3 was also
6 present in the cytoplasm and possibly in the nucleus. Interestingly, accumulation of YFP⁺ axonal
7 debris on the endplate often correlated with the lack of extracellular Gal-3 on neighboring PSCs
8 (Fig. 5C and D, arrows; 6 out of 7 observations). Altogether, these results show that Gal-3 is
9 expressed by PSCs following denervation, is present in the extracellular space at the NMJ and
10 correlates with efficient clearance of presynaptic debris on the endplate.

11

12 *Some PSCs fail to upregulate Gal-3 following denervation in presymptomatic SOD1^{G37R} mice*

13 Based on our Ca²⁺-imaging results, we hypothesized that altered PSCs' decoding
14 properties would be associated with an inadequate phagocytic phenotype on denervated NMJs in
15 presymptomatic SOD1^{G37R} mice. Thus, we tested if PSCs upregulated Gal-3 following an
16 experimentally-induced denervation in presymptomatic SOD1^{G37R} mice (Sciatic nerve crush at
17 ~P180). We evaluated PSCs Gal-3 expression in the EDL (FF NMJs on its surface, (Tremblay et
18 al., 2017)) and the SOL (FR and S NMJs) to assess any MU-type dependent differences. The
19 EDL was used instead of the STM for nerve-crush experiments, since the denervation of SOL
20 and EDL NMJs can be induced using the same surgical procedure (sciatic nerve crush), thereby
21 reducing inter-animal and inter-procedure variability. Furthermore, the surgery to induce the
22 denervation of STM NMJs is much more invasive, causing a strong inflammatory response in the
23 muscle (data not shown) and possibly altering PSC properties. Based on our hypothesis, we

1 predict that PSC Gal-3 expression would be reduced at denervated NMJs of both types in
2 $SOD1^{G37R}$ mice.

3 Interestingly, fewer PSCs upregulated Gal-3 in the EDL and the SOL of P180 $SOD1^{G37R}$
4 mice than of littermate controls two days after sciatic nerve crush (Figure 6A and B, arrows;
5 Figure 6C; WT EDL: N=4, 83 NMJs, n=246 PSCs; WT SOL: N=4, 108 NMJs, n=288 PSCs;
6 $SOD1$ EDL: N=4, 90 NMJs, n=252 PSCs; $SOD1$ SOL: N=4, 89 NMJs, 205 PSCs, Effect of
7 genotype: $p < 0.001$, *GLM*). Importantly, PSC Gal-3 expression was also dependent on the
8 muscle type (Figure 6C, Effect of muscle: $p < 0.001$, *GLM*; Interaction between genotype and
9 muscle: $p = 0.028$, *GLM*) such that significantly fewer PSCs expressed Gal-3 following
10 denervation in the EDL than in the SOL in WT mice (Figure 6C, $74.65 \pm 4.73\%$ vs $88.25 \pm$
11 1.65% respectively, $p = 0.022$, *GLM post-test*) and in $SOD1^{G37R}$ mice (Figure 6C, $42.00 \pm 3.85\%$
12 vs $81.25 \pm 3.01\%$ respectively; $p < 0.001$, *GLM post-test*). Even though more PSCs failed to
13 upregulate Gal-3 in both muscles in $SOD1^{G37R}$ mice compared to WT mice (Figure 6C, EDL:
14 WT vs $SOD1$, $p < 0.001$; SOL: WT vs $SOD1$ $p = 0.022$, *GLM post-test*), this effect was much
15 more pronounced in the EDL than in the SOL. Hence, PSCs seem less likely to adopt a
16 phagocytic phenotype at denervated NMJs in presymptomatic $SOD1^{G37R}$ mice in a manner
17 consistent with NMJ vulnerability in ALS. These results suggest that PSCs may not adequately
18 promote NMJ repair upon the endogenous denervation of NMJs during the symptomatic phase in
19 $SOD1^{G37R}$ mice.

20

21 ***PSC Ca^{2+} activity is no longer altered in the STM of symptomatic $SOD1^{G37R}$ mice***

22 We previously showed that PSC muscarinic receptor activation remained elevated until
23 the pre-onset stage (P380) in the SOL (Arbour et al., 2015). Therefore, we asked if the alteration
24 of PSCs properties at FF NMJs would also persist until the symptomatic stage. To address this

1 question, we first examined PSC Ca^{2+} activity in the STM of phenotypically matched late
2 symptomatic $\text{SOD1}^{\text{G37R}}$ mice and age-matched *WT* mice. PSC Ca^{2+} activity was induced by
3 high-frequency nerve stimulation (50Hz 20 sec) or by local application of muscarine (10 μm) or
4 ATP (1 μm).

5 Among PSCs that met our inclusion criteria (see material and methods), responsiveness
6 to nerve stimulation, local application of muscarine or local application of ATP was similar
7 between groups (Nerve stimulation: $\text{SOD1}^{\text{G37R}}$ 12 out of 12 PSCs, N=5 vs *WT* 13 out of 13 PSCs
8 N=6; Muscarine: $\text{SOD1}^{\text{G37R}}$ 43 out of 52 PSCs, N=8 vs *WT* 33 out of 39 PSCs, N=6 ; ATP:
9 $\text{SOD1}^{\text{G37R}}$ 49 out of 49 PSCs, N=8 vs *WT* 39 out of 39 PSCs, N=6). Although some PSC Ca^{2+}
10 responses to endogenous transmitter release in $\text{SOD1}^{\text{G37R}}$ mice tended to be slightly smaller than
11 in *WT* mice, the difference was not statistically significant (Figure 7A-B; $294.8 \pm 35.7\% \Delta\text{F}/\text{F}_0$,
12 $n=12$ vs $353.4 \pm 31.2\% \Delta\text{F}/\text{F}_0$, $n=13$ respectively; $t_{(23)}=1.227$; $p=0.2324$ *Unpaired t-test*).
13 Similarly, the amplitude of PSC Ca^{2+} responses to local application of muscarine and ATP were
14 similar between *WT* and symptomatic $\text{SOD1}^{\text{G37R}}$ mice (Figure 7C-D; Muscarine : $230.6 \pm 18.8\%$
15 $\Delta\text{F}/\text{F}_0$, $n=33$ vs $233.3 \pm 19.1\% \Delta\text{F}/\text{F}_0$, $n=43$ respectively; $t_{(74)}=1.007$; $p=0.9200$ *Unpaired t-test* ;
16 ATP : $261.8 \pm 16.9\% \Delta\text{F}/\text{F}_0$, $n=39$ vs $288.9 \pm 17.2\% \Delta\text{F}/\text{F}_0$, $n=49$ respectively; $t_{(86)}=1.106$;
17 $p=0.2718$ *Unpaired t-test*). Hence, PSC Ca^{2+} properties seem to have evolved during disease
18 progression in the STM, with Ca^{2+} responses to endogenous transmitter release or local ATP and
19 muscarine applications no longer being reduced in symptomatic $\text{SOD1}^{\text{G37R}}$ mice.

20

21 ***Similar level of denervation in STM and SOL muscles of symptomatic $\text{SOD1}^{\text{G37R}}$ mice***

22 We next wanted to evaluate if PSC's ability to upregulate Gal-3 or to promote NMJ
23 repair was still impaired in symptomatic $\text{SOD1}^{\text{G37R}}$ mice. Using IHC, PSCs' repair properties

1 (Gal-3 expression, PSC process extensions and nerve terminal sprouting) were evaluated at all
2 NMJ types under similar levels of denervation, by comparing the STM and the SOL of
3 phenotypically matched late symptomatic *SOD1^{G37R}* animals (P505-565; Fig. 1A). This
4 experimental design allowed us to isolate the effect of the muscle type on the repair properties
5 since, unlike the STM, denervation levels in leg fast-twitch muscles, such as the EDL, are
6 drastically higher than in the SOL at this stage, with only few NMJs being fully innervated
7 (*unpublished observations* and Tremblay et al. 2017). Observations were analyzed as a function
8 of the innervation state of the NMJs (innervated vs denervated) in addition to the muscle type
9 (STM vs SOL) and the genotype (*WT* vs *SOD1^{G37R}*) as illustrated in Figure 8A.

10 First, we needed to confirm that the level of NMJ denervation in each muscle were
11 comparable. Consistent with previous observations in the *SOD1^{G93A}* mice (Schaefer et al., 2005;
12 Valdez et al., 2012), we confirmed that the extent of denervation (partial or complete) was
13 comparable between the STM and the SOL in symptomatic *SOD1^{G37R}* mice, not being
14 significantly higher in the STM than in the SOL (Fig. 8B; STM: $21.71 \pm 5.76\%$, N=9 vs SOL:
15 $11.51 \pm 1.98\%$, N=7; $p=0.116$; *GLM post-test*). Indeed, we found that $11.63 \pm 3.91\%$ of NMJs in
16 the STM were completely denervated (31 out of 266, N=9) compared to $6.80 \pm 1.84\%$; in the
17 SOL (20 out of 282, N=7). Similar results were obtained for partially denervated NMJs (STM,
18 $10.08 \pm 3.36\%$; 29 out of 266 NMJs, N=9 vs SOL, $4.11 \pm 1.97\%$; 15 out of 282, N=7). Of note,
19 only 1 out of the 156 NMJs analyzed in the STM of *WT* animals ($0.54 \pm 0.54\%$; N=6) was
20 completely denervated and none were partially denervated. In the SOL, none of the 152 NMJs
21 analyzed in *WT* animals (N=5) showed any sign of denervation. A partially denervated NMJ
22 could be either undergoing denervation or re-innervation, which are two very distinct

1 physiological states (Martineau et al., 2018). Due to this uncertainty, partially denervated NMJs
2 were excluded from the following analyses.

3 As intended with this experimental design, these observations confirm that a possible
4 difference in the level of denervation will not bias the analysis of Gal-3 expression or PSC repair
5 properties at symptomatic stage.

6

7 ***Lack of Gal-3 at denervated NMJs in symptomatic SOD1 animals***

8 We examined Gal-3 expression in PSCs NMJs in the STM and the SOL of symptomatic
9 SOD1^{G37R} mice. To rule out age-related changes in the debris clearance pathway (Kang and
10 Lichtman, 2013), we also performed a sciatic nerve crush in aged *WT* mice (P450-P500). PSCs
11 in the SOL of aged *WT* mice robustly expressed Gal-3 following sciatic nerve crush (Fig. 8C;
12 85.03 ± 4.07 %, N=4, n=120) and at similar levels than in P180 mice (Figure 5). Hence, PSCs
13 maintain their ability to upregulate Gal-3 in 14-16 month-old *WT* mice.

14 As expected, we found that PSC Gal-3 expression varied according to the state of
15 innervation and the muscle in SOD1^{G37R} mice and in age-matched controls (Effect of genotype:
16 $p < 0.001$, Effect of innervation: $p < 0.001$, Genotype*innervation interaction: $p < 0.001$;
17 Muscle*innervation interaction: $p < 0.001$, *GLM*). Interestingly however, numerous PSCs did not
18 express Gal-3 on completely denervated NMJs in SOD1^{G37R} mice in both muscles (Fig. 8D₁ and
19 8E₁, arrowheads). Consistent with our finding in presymptomatic mice (Fig. 6), significantly less
20 PSCs expressed Gal-3 in the STM of SOD1^{G37R} animals when compared to nerve crush-induced
21 denervated NMJs in *WT* mice (Fig. 8F; 18.94 ± 8.32 % of PSCs; n=136 vs 85.03 ± 4.07 % of
22 PSCs n=120; $p < 0.001$; *GLM post-test*). Furthermore, presence of Gal-3 was highly variable in
23 the SOL, ranging from 0.00% to 77,78% of PSCs (51.81 ± 13.56 %, n=49), and an overall trend

1 towards lower levels was observed when compared to nerve crush-induced denervation (Fig. 8F;
2 $SOD1^{G37R}$ SOL vs Nerve crush WT SOL; $p=0.074$; *GLM post-test*). Interestingly, PSCs Gal-3
3 expression on denervated NMJs was significantly higher in the SOL than in the STM (Fig. 8F;
4 $SOD1^{G37R}$ SOL vs STM; $p=0.020$; *GLM post-test*), again reflecting the higher vulnerability of FF
5 NMJs. Importantly, axonal SCs in both muscles robustly expressed Gal-3 when associated with
6 denervated NMJs, suggesting that this alteration is specific to PSCs (Fig 8D₁ and E₁). Altogether
7 these results show that PSCs unreliably upregulate Gal-3 on denervated NMJs in symptomatic
8 $SOD1^{G37R}$ mice, especially on vulnerable NMJs.

9
10 ***Gal-3 is expressed on some innervated and partially innervated NMJs in the STM of***
11 ***symptomatic SOD1 mice***

12 Paradoxically, while Gal-3 was absent from PSCs on denervated STM NMJs in
13 $SOD1^{G37R}$ mice, it was expressed in some PSCs on fully innervated NMJs in the STM (Fig. 8D₂,
14 asterisks and 8G; $SOD1^{G37R}$: 12.84 ± 2.54 % of PSCs, n=866 vs WT: 1.55 ± 1.68 % of PSCs,
15 n=618; $p<0.001$; *GLM post-test*). More importantly, a similar proportion of PSCs expressed Gal-
16 3 whether the NMJ was innervated or denervated in the STM of $SOD1^{G37R}$ mice (Fig. 8F-G,
17 12.84 ± 2.54 % vs 18.94 ± 8.32 %; $p=0.132$; *GLM post-test*) suggesting that Gal-3 expression in
18 PSCs was independent of the state of innervation in this ALS model. This upregulation of Gal-3
19 on innervated NMJs was not observed in the SOL of $SOD1^{G37R}$ animals (Fig. 8E₂; $SOD1^{G37R}$
20 SOL Innervated: 3.12 ± 0.92 %, n=708 vs WT SOL Innervated: 2.59 ± 1.50 , n=435 ; $p=0.231$;
21 *GLM post-test*), where its expression was specific to denervated NMJs (Innervated: $3.12 \pm$
22 0.92 % vs Denervated : 51.81 ± 13.56 %; $p<0.001$; *GLM post-test*). Gal-3 expression was also not

1 observed at innervated NMJs in presymptomatic (P120-180) and pre-onset (P350) *SOD1*^{G37R}
2 mice (data not shown).

3 In line with this paradoxical observation, a number of PSCs on partially innervated NMJs
4 also expressed Gal-3 and were usually associated with the nerve terminal in the STM of
5 symptomatic *SOD1*^{G37R} mice (Fig. 9A₁). Again, this was not observed in the SOL (Fig. 9A₂).
6 Indeed, 20 out of 29 (69.97 %) partially innervated NMJs had at least 1 Gal-3⁺-PSC in the STM
7 compared to only 2 out of 15 (13.33 %) in the SOL. In 80% of these cases in the STM Gal-3⁺-PSCs
8 were preferentially associated with the presynaptic nerve terminal. Altogether, these results are
9 suggestive of active PSC phagocytosis of presynaptic elements on denervating or reinnervating
10 NMJs.

11

12 *PSCs extend disorganized processes in both the STM and the SOL*

13 Next, we characterized another fundamental PSC mechanism contributing to NMJ repair:
14 the extension of glial processes and the guidance of terminal sprouting. Importantly, this aspect
15 of PSC repair properties could not be evaluated in presymptomatic animals following a complete
16 nerve crush, since this procedure only poorly induces the extension of PSC processes (Love and
17 Thompson, 1999). We monitored the presence and targeting of PSC process extensions in
18 symptomatic *SOD1*^{G37R} animals. These extensions are normally observed from denervated NMJs
19 towards nearby innervated NMJs, a phenomenon essential in the initiation and guidance of nerve
20 terminal sprouting (Reynolds and Woolf, 1992; Son and Thompson, 1995b, a; Son et al., 1996;
21 O'Malley et al., 1999).

22 In general, we found significantly more NMJs associated with extended PSC processes in
23 *SOD1*^{G37R} than in WT mice (Fig. 10A and B; Effect of genotype: $p < 0.001$, *GLM*) but this effect

1 varied slightly according to the muscle type (Interaction genotype*muscle: $p=0.044$; *GLM*).
2 Denervated NMJs were more likely to be associated with extended PSC processes than
3 innervated NMJs (Effect of innervation: $p<0.001$, *GLM*), but this effect also varied depending on
4 the muscle (Interaction innervation*muscle: $p=0.013$, *GLM*).

5 Indeed, in the STM, completely denervated NMJs were not significantly more likely to
6 be associated with extended PSC processes than innervated NMJs in *SOD1^{G37R}* mice (Fig. 10A₃
7 arrowheads and C; $51.05 \pm 14.99\%$, $n=31$ vs $38.48 \pm 7.11\%$, $n=206$, respectively; $p=0.858$; *GLM*
8 *post-test*). Conversely, innervated NMJs in the STM of *SOD1^{G37R}* mice were more likely to be
9 associated with extended glial processes than innervated NMJs in *WT* mice (Fig. 10A and C,
10 $13.73 \pm 4.05\%$ $n=155$; $p=0.047$; *GLM post-test*). Hence, PSCs in the STM of *SOD1^{G37R}* extended
11 their processes but this did not seem to be dependent on the innervation state of NMJs. These
12 results contrast with those obtained in the SOL. Indeed, PSCs on denervated NMJs in the SOL of
13 *SOD1^{G37R}* mice robustly extended their processes compared to PSCs on innervated NMJs (Fig.
14 10B and C, 71.67 ± 13.76 , $n=36$ vs 15.65 ± 3.68 , $n=247$; $p<0.001$; *GLM post-test*). Hence, while
15 PSC process extensions from denervated NMJs occurred as often in both muscles ($p=0.858$;
16 *GLM post-test*), they were abnormally more likely to be associated with innervated NMJs in the
17 STM than in the SOL ($p=0.047$; *GLM post-test*).

18 Importantly though, these results also show that 49 % of denervated NMJs in the STM
19 and 28% in the SOL lacked PSC process extensions (see Fig.6A₂ for example). These
20 proportions are higher than the expected 1% based on studies using partial denervation (Son and
21 Thompson, 1995b) and, in most cases, only one process per NMJ was observed (1.13 ± 0.67
22 processes on average) (Son and Thompson, 1995b; O'Malley et al., 1999). Furthermore, PSC
23 processes were often highly disorganized in the STM and SOL of *SOD1^{G37R}* mice (47.09 ± 9.87

1 % and 31.02 ± 18.62 % of processes on average respectively; see Fig 10A₃, 10B₂ and 10B₂ for
2 example), often changing direction, not following muscle fibers and frequently making loops
3 around themselves. Hence, although present, PSC process extensions were often disorganized
4 and less abundant than expected on denervated NMJs regardless of the muscle type. These
5 results further suggest that PSC properties are heterogeneous, which is reminiscent of the
6 heterogeneity in PSC decoding properties observed at a presymptomatic stage.

7 8 *Nerve terminal sprouting is absent in the STM and disorganized in the SOL*

9 Extended PSC processes contacting nearby innervated NMJs can initiate and guide nerve
10 terminal sprouting back to denervated NMJs (Son and Thompson, 1995b; Son et al., 1996;
11 O'Malley et al., 1999). However, previous studies reported conflicting results whereby nerve
12 terminal sprouting is absent (Schaefer et al., 2005; Tallon et al., 2016) or abundant in *SOD1*^{G93A}
13 mice (Valdez et al., 2012). Hence, we next tested whether nerve terminal sprouting would be
14 present, albeit disorganized, on innervated NMJs in *SOD1* animals. Based on the lower, but not
15 null, ability of FF NMJs to elaborate terminal sprouts (O'Malley et al., 1999; Frey et al., 2000;
16 Wright et al., 2009), we expected fewer terminal sprouts in the STM compared with the SOL.

17 In general, we found significantly more NMJs associated with nerve terminal sprouts in
18 the SOL of *SOD1*^{G37R} animals than any other groups (Fig. 10A - C; Effect of genotype: $p=0.001$;
19 Effect of muscle: $p<0.001$; Interaction genotype*muscle: $p=0.015$; *GLM*). Indeed, $30.26 \pm 6.96\%$
20 of innervated NMJs in the SOL of *SOD1*^{G37R} mice (Fig. 10B₃; $n=259$) formed sprouts compared
21 to $2.89 \pm 1.46\%$ of SOL NMJs in *WT* mice and $5.26 \pm 1.37\%$ of STM NMJs in *SOD1*^{G37R} mice
22 (Fig. 10A₃, 10B₁ and 10D; $n=152$ and $n=206$, $p<0.001$ and $p<0.001$ respectively; *GLM post-test*)
23 which suggests an active re-innervation effort in the SOL. Consistent with previous observations

1 made on FF NMJs though (Martineau et al., 2018), we did not observe significantly more nerve
2 terminal sprouts at STM NMJs in *SOD1^{G37R}* mice than in *WT* mice ($5.26 \pm 1.37\%$, n=206 vs 2.56
3 $\pm 1.64\%$, n=155; $p=0.311$). This finding was nevertheless surprising considering that over a third
4 of them were being contacted by extended PSC processes (Fig.10A₃ for example). Therefore,
5 initiation of nerve terminal sprouting in symptomatic *SOD1* mice appears deficient in the STM,
6 but not the SOL, resulting in “empty” extended PSCs processes contacting both innervated and
7 denervated endplates (Fig. 10C).

8 Importantly though, nerve terminal sprouts in the SOL were often disorganized, going in
9 many directions and even “avoiding” nearby denervated NMJs (Fig. 10B₂, arrowheads). Indeed,
10 $33.46 \pm 6.50\%$ of sprouting NMJs had disorganized sprouts in the SOL of *SOD1^{G37R}* mice,
11 which is consistent with the muddled PSC process extensions. As a whole, these results show
12 that nerve terminal sprouting was almost completely absent in the STM and disorganized in the
13 SOL of symptomatic *SOD1^{G37R}* animals.

14 In summary, these results show that PSCs display a paradoxical Gal-3 expression in
15 symptomatic *SOD1^{G37R}* animals, being inconsistent on denervated NMJs of both muscles and
16 unexpectedly present on innervated and partially innervated NMJs in the STM. This suggests
17 that PSCs do not adopt a phagocytic phenotype upon denervation of vulnerable NMJs, and also
18 to a lesser extent of partially resistant NMJs. Along with the disorganized processes and the
19 abnormal nerve terminal sprouting, these results suggest that PSCs do not adopt an appropriate
20 phenotype for re-innervation in ALS. Importantly, these main findings were replicated in the
21 STM of a small number of pre-onset (P70) *SOD1^{G93A}* animals. Namely, PSCs on denervated
22 NMJs failed to upregulate Gal-3 and to extend processes, resulting in the absence of nerve

- 1 terminal sprouting (*data not shown*). Altogether, these results show that alteration PSC repair
- 2 properties are not specific to a single *SOD1* model.

1 **DISCUSSION**

2 Our results reveal inappropriate glial repair properties at the NMJs of a fast- and a slow-
3 twitch muscle in symptomatic *SOD1* animals. These changes are associated with an altered PSC
4 excitability, long before disease onset. Despite multiple differences in PSC properties (encoding
5 and repair) between muscles and the heterogeneity in PSC properties, our data converges
6 towards the same end results whereby PSCs on denervated NMJs inconsistently adopted a
7 phagocytic phenotype, formed muddled processes, failed to guide nerve terminal sprouting
8 appropriately and presented an increased mAChR-dependent activity, albeit transiently in a fast
9 twitch muscle. Thus, PSC excitability and repair properties are incompatible with NMJ
10 reinnervation across all MU types in *SOD1* models.

11

12 ***NMJ repair defects in ALS***

13 Here, we show that numerous PSC-dependent NMJ repair mechanisms are abnormal in
14 *SOD1* animals, suggesting that NMJ reinnervation may be deficient during the progression of
15 ALS. Although compensatory reinnervation is known to occur during the disease (Schaefer et al.,
16 2005; Martineau et al., 2018), this process may be suboptimal, resulting in inefficient or unstable
17 NMJ repair. Such bungled compensation could contribute to the loss of motor function in ALS
18 by exacerbating loss of NMJs. Consistent with this hypothesis, numerous studies documented
19 delays in NMJ reinnervation following axonal injury in ALS models (Sharp et al., 2005; Pun et
20 al., 2006; Henriques et al., 2011; Swarup et al., 2012; Mesnard et al., 2013; Carrasco et al.,
21 2016b). These observations suggest that a number of core NMJ repair mechanisms are altered in
22 these models. For instance, an intrinsically slower axonal growth or cellular debris accumulation
23 in the endoneural tube and at the NMJ that would deter NMJ reformation after denervation

1 (Kang and Lichtman, 2013). Our observation that PSCs fail to adopt a phagocytic phenotype on
2 denervated NMJs (Fig. 8) is consistent with these mechanisms. However, since the inadequate
3 Gal-3 expression was specific to PSCs, and was not observed for axonal SCs, our results suggest
4 that other mechanisms besides debris accumulation in the endoneural tube could contribute to the
5 delay in NMJ reinnervation after nerve injury.

6 Importantly, global nerve injuries do not recapitulate the progressive denervation
7 occurring in ALS. Hence, evaluating NMJ repair following partial denervation would be more
8 instructive as it would allow compensatory reinnervation to take place through nodal (axonal)
9 and nerve terminal sprouting of intact motor axons (Thompson and Jansen, 1977; Son and
10 Thompson, 1995b). Since PSCs unreliably extended muddled processes (Fig. 10), we predict that
11 reinnervation based on these sprouting events would also be drastically impaired. Indeed, despite
12 being more abundant than in controls, PSC processes were less abundant than expected (Son and
13 Thompson, 1995b; O'Malley et al., 1999) which could underlie the reduced terminal sprouting
14 observed following blockade of neurotransmission in *SOD1* mice (Frey et al., 2000).
15 Interestingly, Schaefer et al. (2005) and Martineau et al. (2018) observed substantial motor-unit
16 enlargement in the STM during disease progression, but these events appeared to be mostly due
17 to nodal sprouts. This is consistent with the absence or disorganization of nerve terminal sprouts
18 (Fig. 10) and the apparent sparing of axonal SCs documented here (Fig. 8).

19

20 ***Motor-unit type-dependent and independent diversity in PSC properties***

21 Results presented here and previously (Arbour et al., 2015) show (1) that increased
22 mAChR-dependent PSC activity is present long before disease onset, (2) that this alteration is
23 associated with an inability to adopt a phagocytic phenotype upon denervation in

1 presymptomatic animals, and (3) that PSCs' phenotype is incompatible with NMJ repair in
2 symptomatic animals, regardless of the MU-type they are associated with. However, excitability
3 and repair properties of PSCs associated with vulnerable FF MUs (STM) contrasted with those
4 observed on PSCs associated with less vulnerable FR and S MUs (SOL).

5 Indeed, PSC Ca^{2+} signaling is affected differentially depending on the MU-type in
6 *SOD1^{G37R}* mice, revealing a unique set of complementary changes in PSC activity at FF NMJs in
7 contrast with those reported at FR and S MUs (Arbour et al., 2015). For instance, while
8 maintaining a higher relative mAChR contribution, nerve-induced PSC Ca^{2+} responses on FF
9 MUs were smaller, possibly due to a reduced sensitivity of the purinergic system (Fig. 2 and 4).
10 In contrast, PSC Ca^{2+} responses on FR and S MUs were larger due to an increased activation of
11 mAChRs (FR and S) and an increased sensitivity of the purinergic system (FR, pre-onset stage
12 only) (Arbour et al., 2015). This highlights the importance of the balance regulation of PSCs
13 activity between muscarinic and purinergic receptors. A possible explanation for these opposite
14 changes may be linked to the differential MU-specific changes in NMJ activity occurring in
15 *SOD1* mice (Tremblay et al., 2017). Indeed, chronic changes in NMJ activity have been shown
16 to induce plastic changes in PSC properties (Belair et al., 2010).

17 Furthermore, our results suggest that changes in PSC excitability may only be transient
18 on FF NMJs while they seem to become more pronounced at the pre-onset stage on S and FR
19 MUs (Arbour et al., 2015). These results suggest that the altered PSC excitability may also
20 confer some benefits on NMJ stability (i.e. before it denervates). Alternatively, but not
21 exclusively, transient changes in PSC excitability may reflect longer-lasting changes in PSC
22 function. Further examination of PSC excitability on denervated NMJs in symptomatic *SOD1*
23 mice could shed light on this question. Unfortunately, nerve-muscle preparations from

1 symptomatic *SOD1* animals are more fragile and PSCs on denervated NMJs seem more
2 vulnerable to the AM loading procedure (Arbour et al., 2015). Future investigation of PSC
3 properties using another approach, such as GCaMP expression (Heredia et al., 2018), may
4 potentially circumvent those limitations.

5 Moreover, PSC repair properties varied according to the MU type in symptomatic
6 *SOD1^{G37R}* animals, where PSC properties on FF NMJs were out of phase with the innervation
7 status while PSCs on FR or S NMJs adopted a less pronounced phenotype. Similarly, the
8 expression of the chemorepellent Semaphorin 3A was selectively increased in FF NMJs
9 following denervation or blockage of neurotransmitter release (De Winter et al., 2006). All these
10 results are consistent with the known vulnerability of FF MUs compared to FR and S MUs in the
11 disease (Frey et al., 2000; Atkin et al., 2005; Pun et al., 2006). Importantly, these differences
12 were not due to STM being further along the progression of the disease than the SOL considering
13 that denervation levels were comparable between the STM and the SOL at this stage. Hence,
14 PSC repair properties reflect MU vulnerability at presymptomatic and symptomatic stages of the
15 disease. Furthermore, the lack of PSC-dependent synaptic repair at FF NMJs could contribute to
16 their increased vulnerability in ALS.

17 An additional level of complexity arises from the increased heterogeneity in PSC activity
18 (nerve-induced Ca^{2+} -responses) and repair properties (Gal-3 expression and process extensions)
19 at individual NMJs in *SOD1* animals. Heterogeneity in PSC responses to synaptic activity could
20 arise from two scenarios. First, a mAChR-independent component of PSC Ca^{2+} responses could
21 be inconsistently decreased amongst PSCs. Second, knowing that PSCs cover exclusive synaptic
22 territories (Brill et al., 2011) and that synaptic activity is altered at the NMJ in ALS (Armstrong
23 and Drapeau, 2013b, a; Rocha et al., 2013; Shahidullah et al., 2013; Arbour et al., 2015;

1 Tremblay et al., 2017), neurotransmitter release could be more heterogeneous between active
2 zones, thus inducing variable levels of Ca^{2+} activity in PSCs depending on the active zones they
3 cover.

4 Altogether, common pathological alterations in PSC properties are complemented by
5 numerous context-dependent differences that could contribute to, or at least reflect, NMJ
6 dysfunction and MU-vulnerability in ALS.

7 *Non-cell autonomy at the NMJ and impact of PSC dysfunction on disease progression.*

8 Similarly to glial cells in the CNS (Boillee et al., 2006a; Boillee et al., 2006b; Yamanaka
9 et al., 2008; Ilieva et al., 2009; Haidet-Phillips et al., 2011; Kang et al., 2013; Meyer et al., 2014;
10 Ditsworth et al., 2017), results presented here and in recent studies (Carrasco et al., 2016a; Van
11 Dyke et al., 2016), suggest that alterations in PSC properties could contribute to ALS onset and
12 progression. Direct manipulation of mutant SOD1 levels in astrocytes, microglia or
13 oligodendrocyte progenitors directly affected their function and revealed their contribution to the
14 disease. These results raise the question of whether changes in PSCs are directly caused by the
15 expression of the mutant protein or reflect a maladaptive response to the diseased motoneuron.
16 Previous studies evaluating the contribution of mutant SOD1 expression in SCs (both PSCs and
17 axonal SCs) to the disease provided disparate results depending on the dismutase competency of
18 the mutated SOD1 protein (Lobsiger et al., 2009; Turner et al., 2010; Wang et al., 2012).
19 However, the P0 promoter used in these studies poorly targets PSCs (Lobsiger et al., 2009).
20 Furthermore, we show here that axonal SCs robustly adopted a phagocytic phenotype following
21 denervation in symptomatic *SOD1* mice, while PSCs failed to do so (Fig. 8), suggesting that
22 different types of Schwann cells may be affected differently in the disease. Unfortunately, lack of

1 a known specific PSC promoter has so far prevented a direct manipulation of mutant SOD1
2 expression in PSCs. Interestingly, Castro et al. (2020) recently suggested a genetic strategy to
3 identify PSCs which could open the possibility to develop new tools to target them selectively.
4 Hence, the contribution of mutant SOD1 expression in PSCs to their dysfunction and to ALS
5 onset and progression remains to be determined.

6

7 ***Role of Gal-3 in ALS***

8 Numerous studies have evaluated the role of Galectin-3 (MAC-2) in ALS and its
9 usefulness as a potential biomarker for the disease (Zhou et al., 2010). For instance, Gal-3
10 expression is increased early in the spinal cord of *SOD1^{G93A}* mice and ALS patients, in skeletal
11 muscles of *SOD1^{G86R}* mice (possibly in axonal SCs based on our results), and rises throughout
12 disease progression (Ferraiuolo et al., 2007; Gonzalez de Aguilar et al., 2008; Zhou et al., 2010;
13 Lerman et al., 2012; Baker et al., 2015). Its expression correlates with microglial activation
14 (Yamanaka et al., 2008; Lerman et al., 2012) and is also inexplicably upregulated in
15 motoneurons during disease progression (Ferraiuolo et al., 2007). These observations have been
16 interpreted as indications that Gal-3 expression could play a detrimental role in disease
17 progression or would at least reflect increasing levels of neuroinflammation.

18 However, Gal-3 has been implicated in numerous cellular functions which could be
19 protective in ALS (Dumic et al., 2006; Yang et al., 2008) such as phagocytosis in astrocytes
20 (Nguyen et al., 2011; Baker et al., 2015; Morizawa et al., 2017) and myelin phagocytosis in
21 axonal SCs (Reichert et al., 1994). Although still debated, evidence suggest it could play a
22 similar role in microglia (Rotshenker, 2009; Lalancette-Hebert et al., 2012). These results
23 suggest that its upregulation may be linked to increased cellular debris clearance in ALS. Our

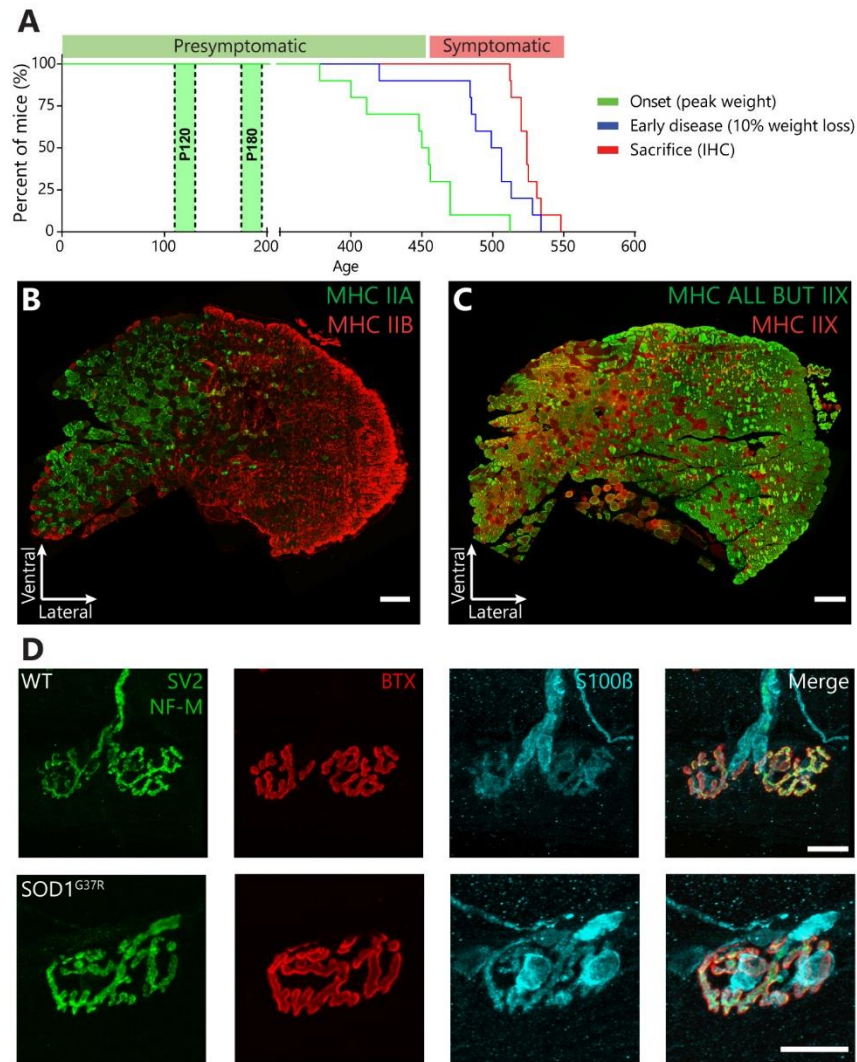
1 results suggest that extracellular Gal-3 at the NMJ and in peripheral nerves would exert a
2 beneficial effect on disease progression, being inversely correlated to the accumulation of axonal
3 debris. However, a role of intracellular Gal-3 cannot be cast out as both fractions could not be
4 labeled simultaneously. Lack of debris clearance would delay NMJ reinnervation (Kang and
5 Lichtman, 2013) causing PSCs to gradually abandon parts of the endplate, thus leading to
6 incomplete NMJ reinnervation (Kang et al., 2014). In agreement with this possibility, crossing
7 *SOD1^{G93A}* mice to Gal-3 knock-out (*lgal3^{-/-}*) mice significantly accelerated disease progression
8 (Lerman et al., 2012), further supporting a protective role of Gal-3 in ALS. Overall, these results
9 suggest that the effect of Gal-3 in ALS is context-specific, exerting different adaptive or
10 maladaptive roles in different cell types.

11

12 ***Conclusion***

13 We show that PSC excitability and repair properties are incompatible with NMJ repair
14 across all MU types, in two *SOD1* ALS mice models, in a manner which reflects their selective
15 vulnerability. These results suggest that compensatory NMJ reinnervation may be defective in
16 ALS due to misguided nerve terminal sprouting and inadequate endplate debris clearance.
17 Further studies aimed at understanding the molecular basis of the diversity and the changes in
18 PSCs in ALS could unravel novel therapeutic targets. Restoring PSCs' repair capabilities could
19 enhance synaptic reestablishment which could improve motor function in ALS patients.

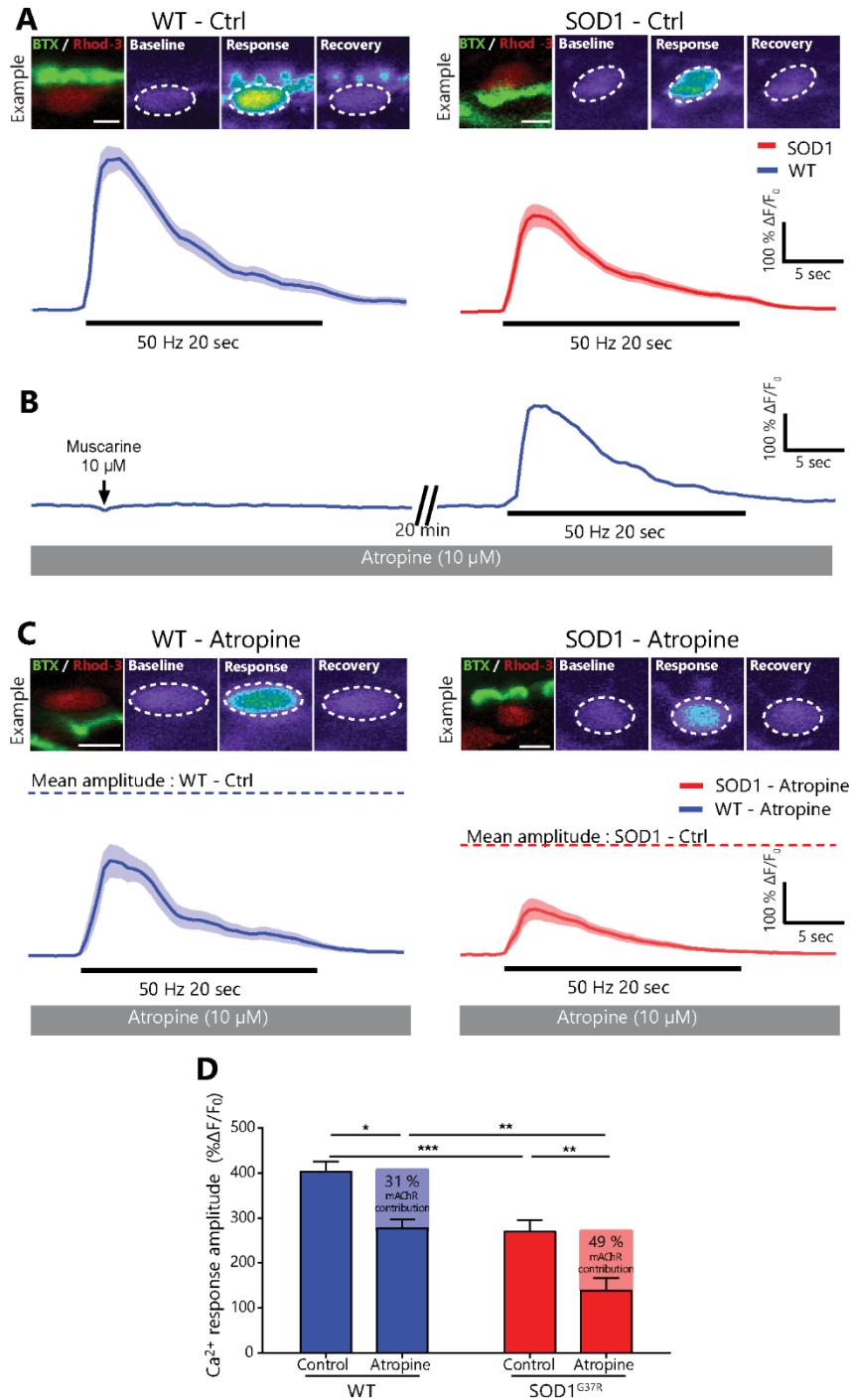
1 FIGURES AND LEGENDS



2

3 **Figure 1: Disease progression in *SOD1*^{G37R} mice and fiber type composition of the**
4 ***Sternomastoid* muscle. (A)** Kaplan-Meier plot of the ages at which disease onset (green; median
5 age: 456 days) and early disease (blue; median age: 506 days) are reached in *SOD1*^{G37R} mice
6 under our conditions. All the symptomatic animals displayed similar motor phenotypes and were
7 sacrificed (red, median 527 days) after the early disease stage. Experiments on presymptomatic
8 animals were carried at P120 and P180. **(B-C)** Immunostaining of *Sternomastoid* cross-sections
9 for Myosin Heavy Chain (MHC) type Iib (FF, red) and Iia (FR, green) (B) or all isotypes except

- 1 Iix (all but Iix, green) and type Iix (FF, red) (C). Scale bars = 200 μm . **(D)** Representative
- 2 examples of presynaptic nerve terminals (green, SV2 and NF-M), postsynaptic nAChR receptors
- 3 red, (α -BTX) and glia (blue; S100 β) labeling from the STM of P120 *WT* and *SOD1^{G37R}* mice.
- 4 Scale bars = 20 μm .
- 5

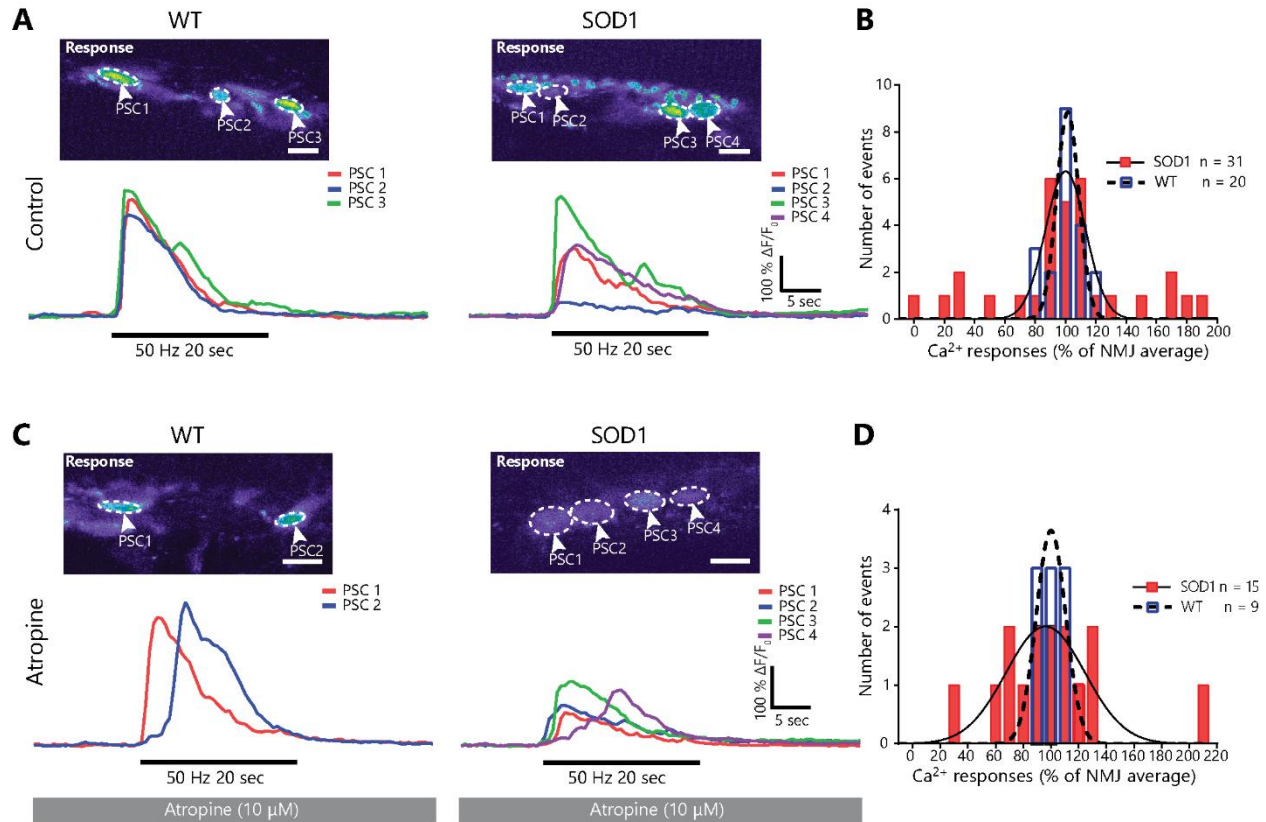


1

2 **Figure 2: Relative increase of mAChR-dependent PSC activity in *SOD1*^{G37R} mice at a**
 3 **presymptomatic stage. (A) Average PSC Ca²⁺ responses ± SEM (pale area) in *SOD1*^{G37R} mice**
 4 **(right) and WT controls (left) induced by high-frequency nerve stimulation at P180 in absence of**

1 atropine (Ctrl). *Top*, localization of the PSC on an endplate (left, apposed over BTX staining)
2 and representative false color images of the changes in Rhod-3 fluorescence representing
3 changes in intracellular Ca^{2+} levels before, during and after motor nerve stimulation. **(B)**
4 Example of PSC Ca^{2+} responses in *WT* controls evoked by local application of muscarine (*left*) or
5 nerve stimulation (*right*) in presence of 10 μM atropine. Note the blockade of muscarine-induced
6 Ca^{2+} response and the reduced amplitude of nerve stimulation-evoked Ca^{2+} responses (*left*,
7 compared with **A**). **(C)** Average PSC Ca^{2+} responses \pm SEM (pale area) in *SOD1*^{G37R} mice (*right*)
8 and *WT* controls (*left*) induced by high-frequency nerve stimulation at P180 in presence of 10
9 μM atropine. Note the reduced amplitude of nerve stimulation-evoked Ca^{2+} responses compared
10 with the average peak amplitude without atropine (dashed lines) *Top*, localization of the PSC on
11 an endplate (left) and representative false color images of the changes in Rhod-3 fluorescence
12 representing changes in Ca^{2+} levels before, during and after motor nerve stimulation. **(D)**
13 Histogram of the amplitude of PSC Ca^{2+} responses in all conditions P180. Scale bar = 5 μm . *, p
14 <0.05; **, p <0.01; ***, p <0.005.

15



1

2 **Figure 3: Muscarinic receptor-independent heterogeneity in PSC activity at individual**

3 **NMJs in the STM of presymptomatic *SOD1*^{G37R} animals. (A) Examples of PSC Ca²⁺**

4 **responses from a single NMJ in *SOD1*^{G37R} mice (right) and WT controls (left) in absence of**

5 **Atropine. Note the greater heterogeneity in Ca²⁺ responses in *SOD1*^{G37R} mice. (B) Frequency**

6 **distribution of PSC Ca²⁺ in WT (blue, dashed line) and *SOD1*^{G37R} (red, solid line) mice**

7 **normalized to the average response of all PSCs on their NMJ. (C) Example of individual PSC**

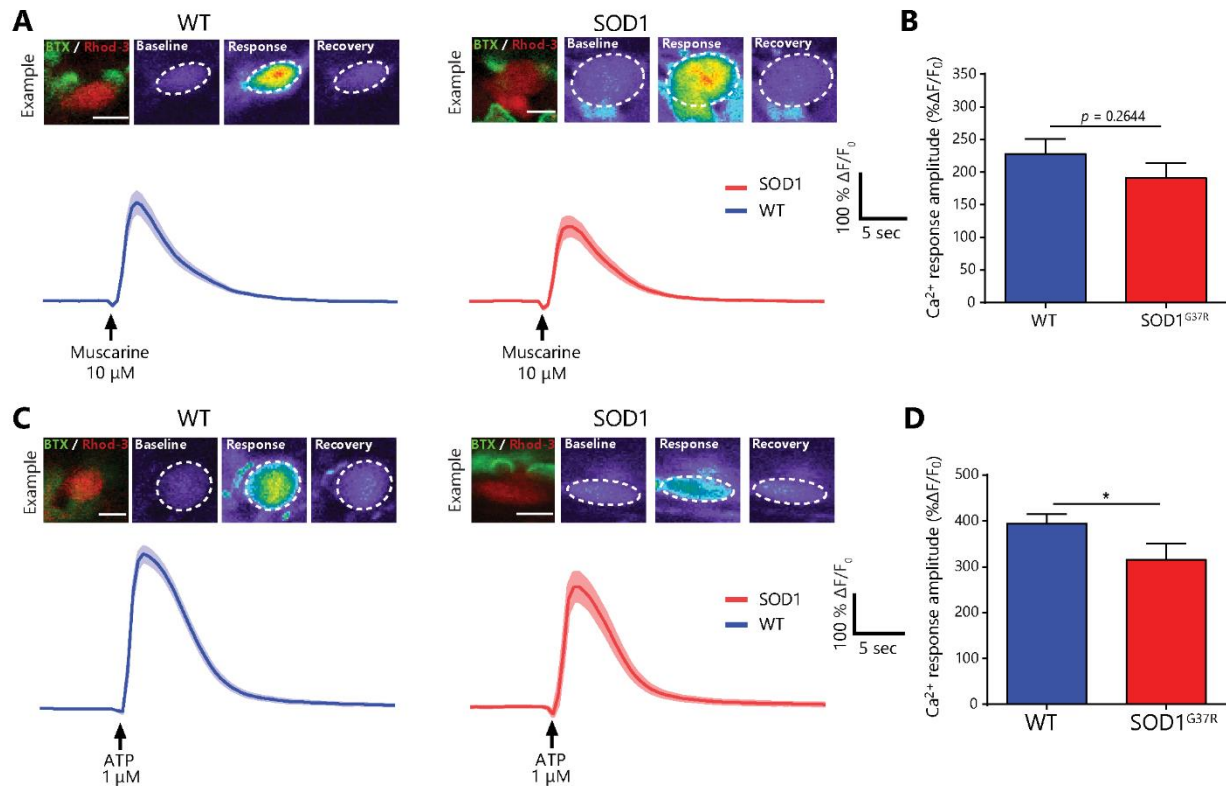
8 **Ca²⁺ responses from an NMJ in *SOD1*^{G37R} mice (right) and WT controls (left) in presence of**

9 **Atropine. (D) Frequency distribution of PSC Ca²⁺ in WT (blue, dashed line) and *SOD1*^{G37R} (red,**

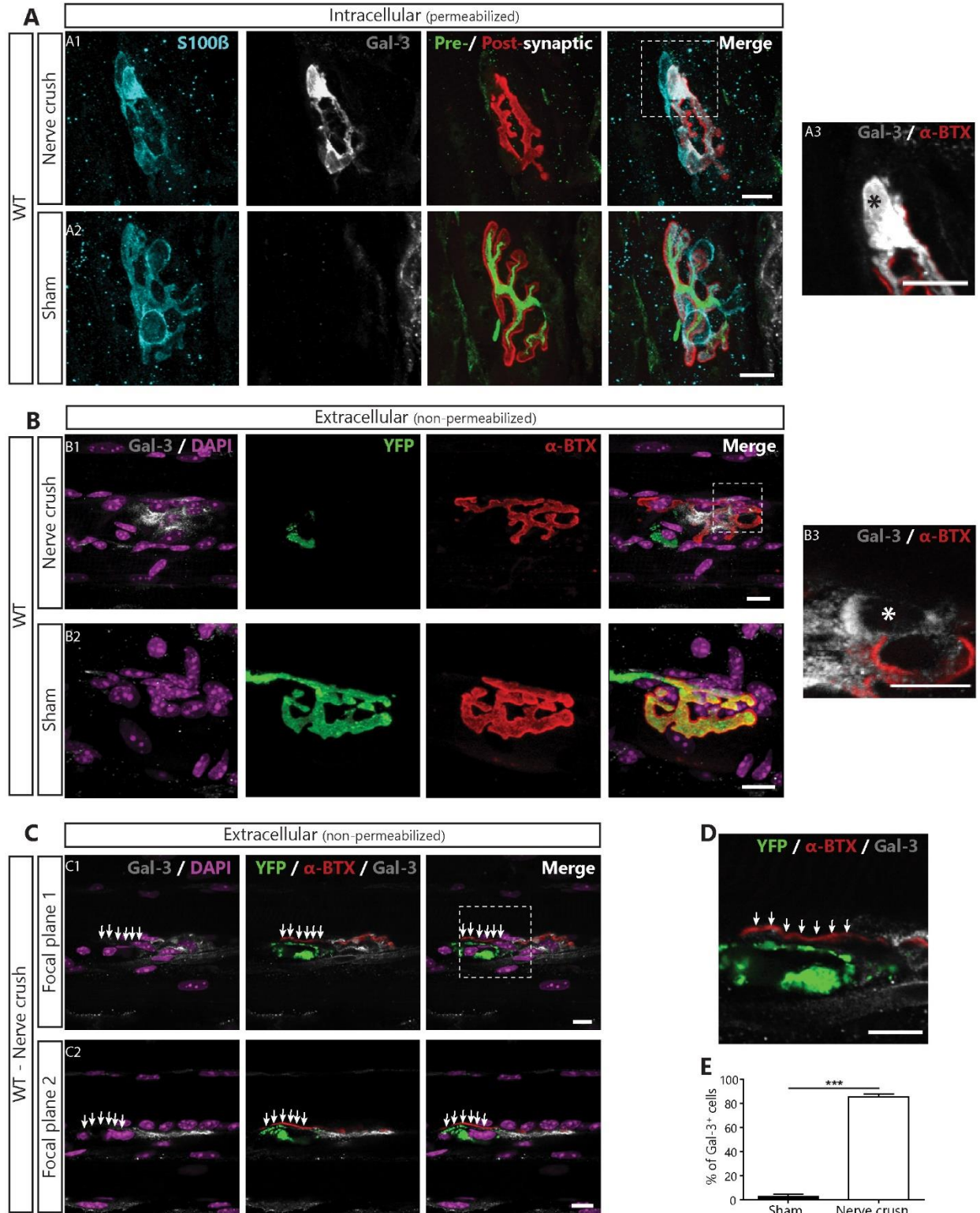
10 **solid line) mice normalized to the average response of all PSCs on their NMJ in presence of**

11 **atropine. Lines in B and C represent best-fit Gaussian curves for each sample (WT: dashed line;**

12 ***SOD1*^{G37R}: solid line) and are used for representation purposes only. Scale bar = 10 μ m.**



1
 2 **Figure 4: PSC Ca²⁺ responses elicited by local application of muscarine or ATP in**
 3 **presymptomatic *SOD1*^{G37R} mice. (A) Average PSC Ca²⁺ responses \pm SEM (pale area) in**
 4 ***SOD1*^{G37R} mice (right) and WT controls (left) induced by local application of muscarine at P180.**
 5 **Top, localization of the PSC on an endplate (left, apposed over BTX staining) and representative**
 6 **false color images of the changes in Rhod-3 fluorescence representing changes in intracellular**
 7 **Ca²⁺ levels before, during and after the response. (B) Histogram of the amplitude of PSC Ca²⁺**
 8 **responses induced by muscarine application at P180. (C) Average PSC Ca²⁺ responses \pm SEM**
 9 **(pale area) in *SOD1*^{G37R} mice (right) and WT controls (left) induced by local application of ATP**
 10 **at P180. Top, localization of the PSC on an endplate and representative false color images of the**
 11 **changes in Rhod-3 fluorescence representing changes in Ca²⁺ levels before, during and after the**
 12 **response. (D) Histogram of the amplitude of PSC Ca²⁺ responses induced by ATP application at**
 13 **P180. Scale bar = 5 μ m. *, $p < 0.05$.**

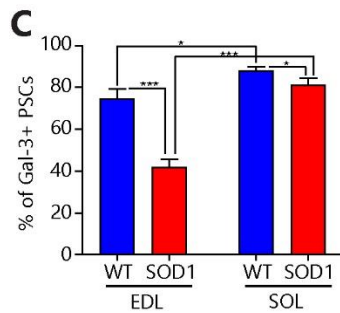
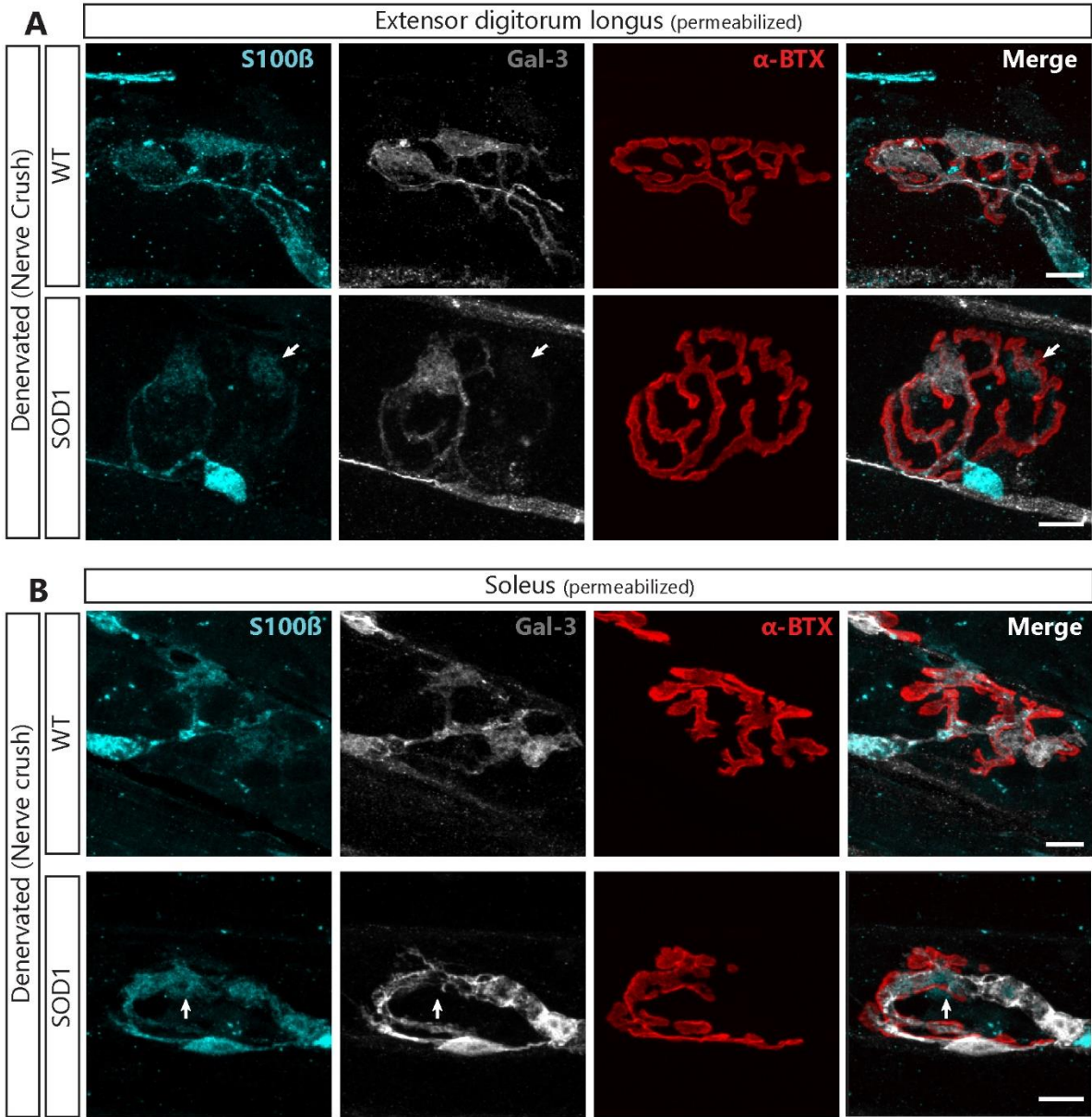


1

2

1 **Figure 5: PSCs express the phagocytic marker Gal-3 following denervation.**
2 **(A)** Representative confocal images of immunolabeling of glial cells (blue; S100 β), Gal-3
3 (white), presynaptic nerve terminals and postsynaptic nAChR (merged: respectively green, SyT;
4 red, α -BTX,) from the SOL of *WT* mice following a sciatic nerve crush (A1), or in Sham
5 operated animal (A2). (A3) High magnification image of the region identified in A1 showing
6 that Gal-3 is present inside the soma (*). **(B)** Representative images of the extracellular labelling
7 of postsynaptic nAChR (red), Gal-3 (white) and nuclei (DAPI; purple) from the SOL of Thy1-
8 YFP mice following sciatic nerve crush (B1) or Sham surgery (B2). (B3) High magnification
9 image of the region identified in B1 showing that Gal-3 is present around the soma (*). Note that
10 Gal-3 appears to be both intracellular and extracellular following NMJ denervation. **(C)** Two
11 single confocal planes of a denervated NMJ showing that YFP⁺-debris accumulation on the
12 endplate (arrows) correlates with the lack of extracellular Gal-3 following sciatic nerve crush.
13 **(D)** High magnification of the region in C1 showing that Gal-3 is absent next to YFP⁺-debris. **(E)**
14 Percentage of PSCs expressing Gal-3. Quantification is based on permeabilized immunolabeling.
15 Scale bar = 10 μ m. ***, p<0.005.

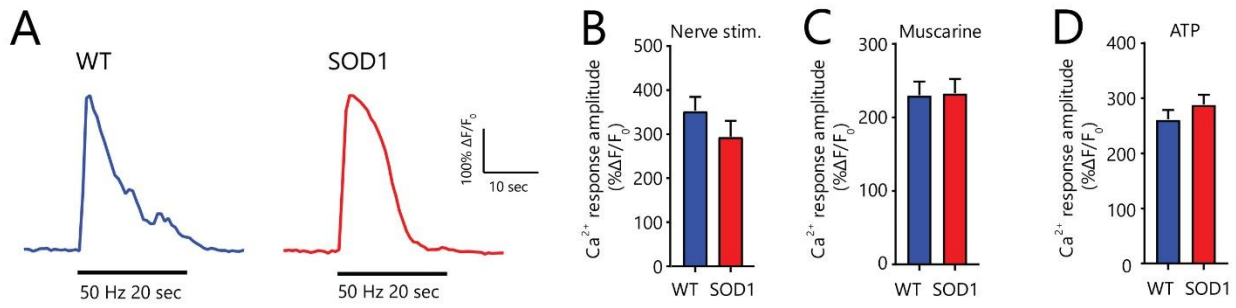
16



1 **Figure 6: Lower expression of Gal-3 in PSCs of presymptomatic *SOD1^{G37R}* mice following**
2 **denervation.** Representative confocal images of the immunolabeling of glial cells (blue; S100 β),
3 Gal-3 (white) and postsynaptic nAChR (red, α -BTX,) from the EDL (**A**) or the SOL (**B**) of *WT*
4 (top) and *SOD1^{G37R}* mice (bottom) two days after a sciatic nerve crush. Note the absence of Gal-
5 3 expression in some of the PSCs from *SOD1* mice (arrows). (**C**) Quantification of the
6 percentage of PSCs expressing Gal-3 two days following a sciatic nerve crush as a function of
7 the genotype and the muscle type. Scale bar = 10 μ m. *, $p < 0.05$; ***, $p < 0.001$.

8

1



2

3 **Figure 7: Unchanged PSC properties in phenotypically-matched symptomatic *SOD1*^{G37R}**

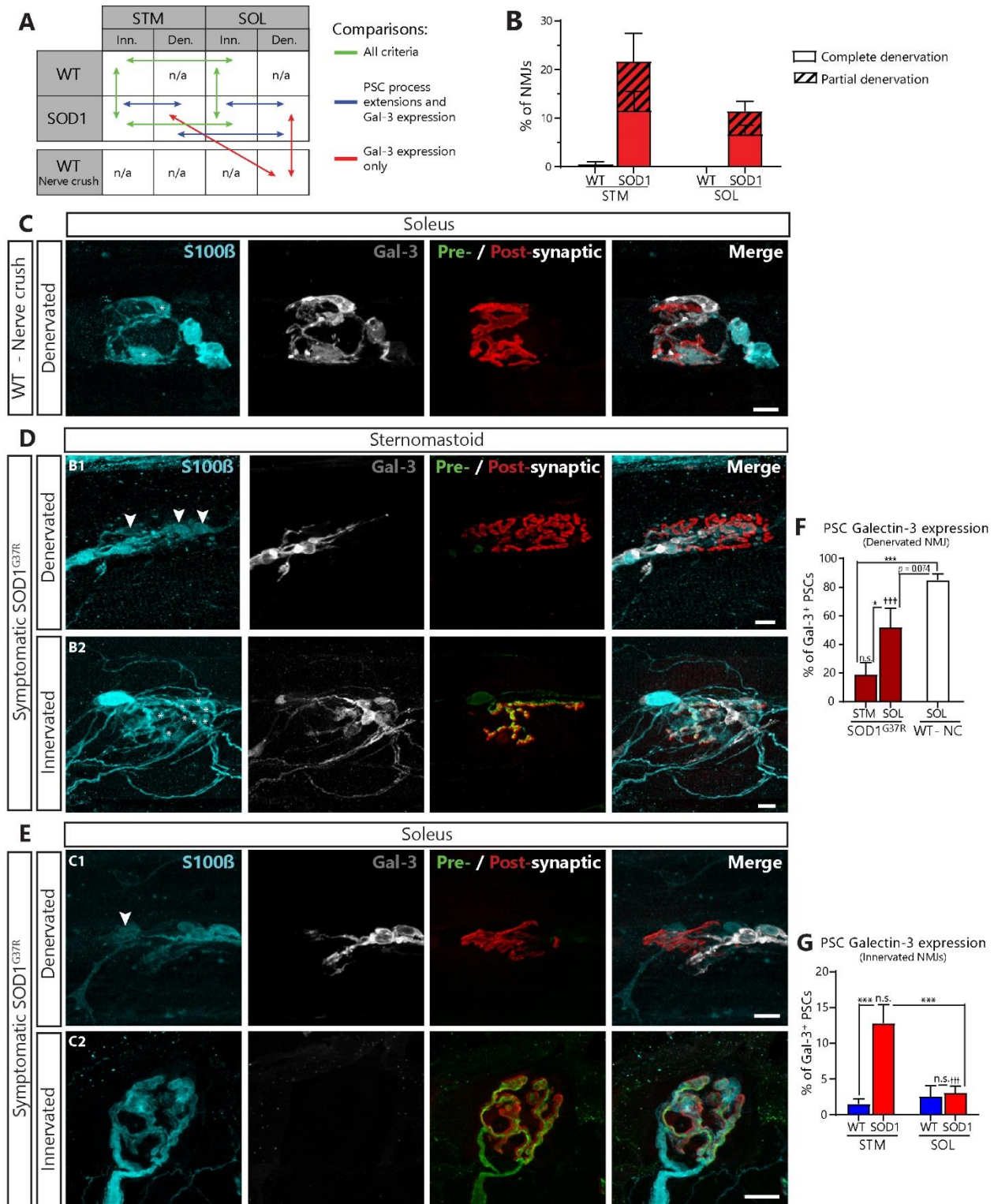
4 **mice. (A)** Representative examples of PSC Ca²⁺ responses induced by high-frequency nerve

5 stimulation in *WT* (blue) and *SOD1*^{G37R} (red) mice. **(B-D)** Histograms of the amplitude of PSC

6 Ca²⁺ responses induced by high-frequency nerve stimulation **(B)** and local application of 10μM

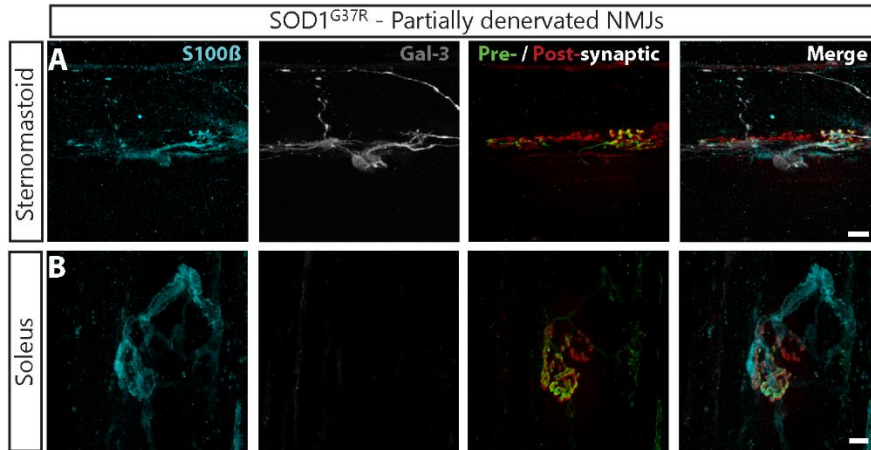
7 muscarine **(C)** or 1 μM ATP **(D)**.

8



1
2 **Figure 8: Paradoxical expression of Gal-3 in the STM and SOL of symptomatic *SOD1*^{G37R}**
3 **mice. (A)** Schematic of the biologically relevant pairwise comparisons to assess the effect of
4 genotype (*WT* vs *SOD1*^{G37R}), muscle type (STM vs SOL) and innervation status (innervated vs

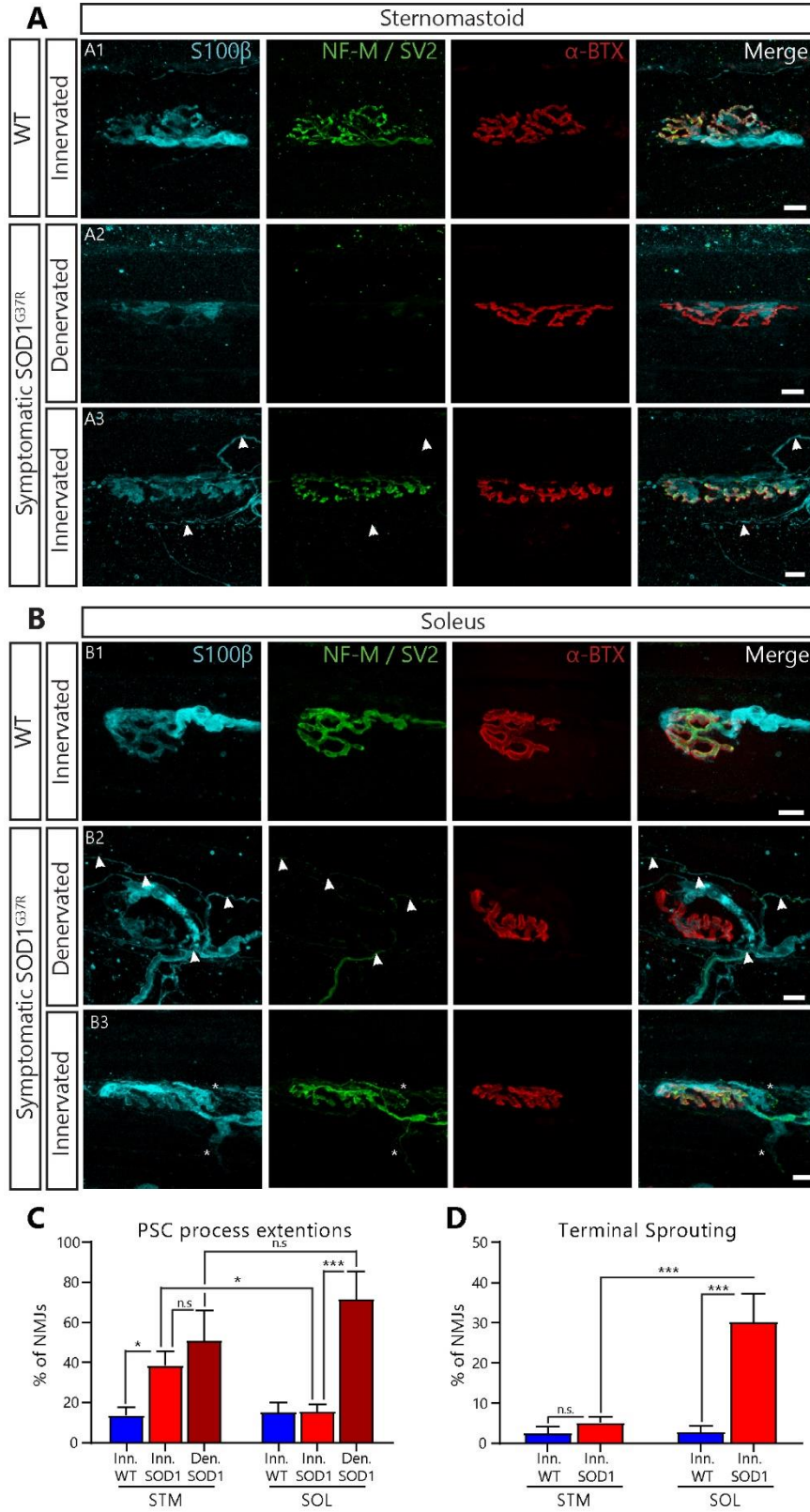
1 denervated). **(B)** Histogram of the percentage of completely and partially denervated NMJs
2 across all groups. Den., denervated; Inn., innervated. **(C-E)** Immunolabeling of glia (blue;
3 S100 β), Gal-3 (white), presynaptic nerve terminals and postsynaptic nAChR receptors (merged:
4 respectively green, SV2 and NF-M; red, α -BTX). **(C)** Representative confocal images of NMJs
5 from the SOL of aged *WT* mice following nerve-crush induced denervation. **(D)** Representative
6 confocal images of denervated (B1) and innervated (B2) NMJs from the STM of symptomatic
7 *SODI^{G37R}* mice. Note the presence of Gal-3 in PSCs (*) on an innervated NMJ in the STM of
8 *SODI^{G37R}* mice. Also note the disorganization of PSC processes. **(E)** Representative confocal
9 images of denervated (C1) and innervated (C2) NMJs from the SOL of *SODI^{G37R}* mice. Note the
10 presence of Gal-3 in axonal Schwann cells and its absence from PSCs (B and C, arrowheads).
11 **(F)** Percentage of PSCs expressing Gal-3 on denervated NMJs and, **(G)** innervated NMJs in all
12 groups. Symbols on the top of histogram bars represent the difference between innervated and
13 denervated NMJs (D vs E). Scale bars = 10 μ m. ns, nonsignificant; ***, $p < 0.005$; †††, $p < 0.005$.
14



1

2 **Figure 9: Gal-3 in PSCs associated with nerve terminals on partially innervated NMJs in**
3 **the STM of symptomatic *SOD1^{G37R}* mice.** Immunolabeling of glia (blue; S100β), Gal-3
4 (white), presynaptic nerve terminals and postsynaptic nAChR receptors (merged: respectively
5 green, SV2 and NF-M; red, α-BTX). **(A)** Representative confocal images of partially innervated
6 NMJs from the STM and **(B)** the SOL of symptomatic *SOD1^{G37R}* mice. Note that Gal-3⁺-PSCs
7 are preferentially associated with the innervated part of the endplate rather than the denervated
8 part. Scale bars = 10 μm

9



1 **Figure 10: Abnormal and disorganized nerve terminal sprouting and PSC process**
2 **extension in the STM and the SOL of symptomatic *SODI*^{G37R} mice.** Immunolabeling of glial
3 cells (blue; S100β), presynaptic nerve terminals (green; NF-M and SV2) and postsynaptic
4 nAChR receptors (red; α-BTX). **(A)** Representative confocal images of NMJs from the STM of
5 age-matched *WT* controls (A1) and of symptomatic *SODI*^{G37R} mice (A2: denervated; A3:
6 innervated). **(B)** Representative confocal images of NMJs from the SOL of *WT* animals (B1) and
7 of symptomatic *SODI*^{G37R} mice (B2: denervated; B3: innervated). Note the nerve terminal
8 sprouting “avoiding” the nearby denervated NMJ (B2; arrowheads). **(C)** The percentage of NMJs
9 associated with PSC processes in the STM or the SOL according to the state of innervation. **(D)**
10 Percentage of innervated NMJs displaying nerve terminal sprouting. Scale bars = 10 μm. ns,
11 nonsignificant; *, $p < 0.05$; ***, $p < 0.005$.

12

1 REFERENCES

- 2 Arbour D, Vande Velde C, Robitaille R (2017) New perspectives on amyotrophic lateral sclerosis:
3 the role of glial cells at the neuromuscular junction. *J Physiol* 595:647-661.
- 4 Arbour D, Tremblay E, Martineau E, Julien JP, Robitaille R (2015) Early and Persistent Abnormal
5 Decoding by Glial Cells at the Neuromuscular Junction in an ALS Model. *J Neurosci*
6 35:688-706.
- 7 Armstrong GA, Drapeau P (2013a) Loss and gain of FUS function impair neuromuscular synaptic
8 transmission in a genetic model of ALS. *Hum Mol Genet* 22:4282-4292.
- 9 Armstrong GA, Drapeau P (2013b) Calcium channel agonists protect against neuromuscular
10 dysfunction in a genetic model of TDP-43 mutation in ALS. *J Neurosci* 33:1741-1752.
- 11 Atkin JD, Scott RL, West JM, Lopes E, Quah AK, Cheema SS (2005) Properties of slow- and fast-
12 twitch muscle fibres in a mouse model of amyotrophic lateral sclerosis. *Neuromuscul*
13 *Disord* 15:377-388.
- 14 Baker DJ, Blackburn DJ, Keatinge M, Sokhi D, Viskaitis P, Heath PR, Ferraiuolo L, Kirby J, Shaw PJ
15 (2015) Lysosomal and phagocytic activity is increased in astrocytes during disease
16 progression in the SOD1 (G93A) mouse model of amyotrophic lateral sclerosis. *Front Cell*
17 *Neurosci* 9:410.
- 18 Belair EL, Vallee J, Robitaille R (2010) In vivo long-term synaptic plasticity of glial cells. *The*
19 *Journal of physiology* 588:1039-1056.
- 20 Boillee S, Vande Velde C, Cleveland DW (2006a) ALS: a disease of motor neurons and their
21 nonneuronal neighbors. *Neuron* 52:39-59.
- 22 Boillee S, Yamanaka K, Lobsiger CS, Copeland NG, Jenkins NA, Kassiotis G, Kollias G, Cleveland
23 DW (2006b) Onset and progression in inherited ALS determined by motor neurons and
24 microglia. *Science* 312:1389-1392.
- 25 Brichta AM, Callister RJ, Peterson EH (1987) Quantitative analysis of cervical musculature in
26 rats: histochemical composition and motor pool organization. I. Muscles of the spinal
27 accessory complex. *J Comp Neurol* 255:351-368.
- 28 Brill MS, Lichtman JW, Thompson W, Zuo Y, Misgeld T (2011) Spatial constraints dictate glial
29 territories at murine neuromuscular junctions. *The Journal of cell biology* 195:293-305.
- 30 Brosius Lutz A, Chung WS, Sloan SA, Carson GA, Zhou L, Lovelett E, Posada S, Zuchero JB, Barres
31 BA (2017) Schwann cells use TAM receptor-mediated phagocytosis in addition to
32 autophagy to clear myelin in a mouse model of nerve injury. *Proc Natl Acad Sci U S A*
33 114:E8072-E8080.
- 34 Carrasco DI, Seburn KL, Pinter MJ (2016a) Altered terminal Schwann cell morphology precedes
35 denervation in SOD1 mice. *Exp Neurol* 275 Pt 1:172-181.
- 36 Carrasco DI, Bahr BA, Seburn KL, Pinter MJ (2016b) Abnormal response of distal Schwann cells
37 to denervation in a mouse model of motor neuron disease. *Exp Neurol* 278:116-126.
- 38 Castro R, Taetzsch T, Vaughan SK, Godbe K, Chappell J, Settlage R, Valdez G (2020) Identification
39 of a molecular fingerprint for synaptic glia. *bioRxiv*.
- 40 Crawley MJ (2007) *The R book*. Chichester, England ; Hoboken, N.J.: Wiley.
- 41 Darabid H, Arbour D, Robitaille R (2013) Glial cells decipher synaptic competition at the
42 mammalian neuromuscular junction. *The Journal of neuroscience : the official journal of*
43 *the Society for Neuroscience* 33:1297-1313.

- 1 De Winter F, Vo T, Stam FJ, Wisman LA, Bar PR, Niclou SP, van Muiswinkel FL, Verhaagen J
2 (2006) The expression of the chemorepellent Semaphorin 3A is selectively induced in
3 terminal Schwann cells of a subset of neuromuscular synapses that display limited
4 anatomical plasticity and enhanced vulnerability in motor neuron disease. *Molecular*
5 *and cellular neurosciences* 32:102-117.
- 6 Ditsworth D, Maldonado M, McAlonis-Downes M, Sun S, Seelman A, Drenner K, Arnold E, Ling
7 SC, Pizzo D, Ravits J, Cleveland DW, Da Cruz S (2017) Mutant TDP-43 within motor
8 neurons drives disease onset but not progression in amyotrophic lateral sclerosis. *Acta*
9 *Neuropathol* 133:907-922.
- 10 Dumic J, Dabelic S, Flogel M (2006) Galectin-3: an open-ended story. *Biochim Biophys Acta*
11 1760:616-635.
- 12 Duregotti E, Negro S, Scorzeto M, Zornetta I, Dickinson BC, Chang CJ, Montecucco C, Rigoni M
13 (2015) Mitochondrial alarmins released by degenerating motor axon terminals activate
14 perisynaptic Schwann cells. *Proc Natl Acad Sci U S A* 112:E497-505.
- 15 Eisen A, Kiernan M, Mitsumoto H, Swash M (2014) Amyotrophic lateral sclerosis: a long
16 preclinical period? *J Neurol Neurosurg Psychiatry* 85:1232-1238.
- 17 Feng G, Mellor RH, Bernstein M, Keller-Peck C, Nguyen QT, Wallace M, Nerbonne JM, Lichtman
18 JW, Sanes JR (2000) Imaging neuronal subsets in transgenic mice expressing multiple
19 spectral variants of GFP. *Neuron* 28:41-51.
- 20 Ferraiuolo L, Heath PR, Holden H, Kasher P, Kirby J, Shaw PJ (2007) Microarray analysis of the
21 cellular pathways involved in the adaptation to and progression of motor neuron injury
22 in the SOD1 G93A mouse model of familial ALS. *J Neurosci* 27:9201-9219.
- 23 Fischer LR, Culver DG, Tennant P, Davis AA, Wang M, Castellano-Sanchez A, Khan J, Polak MA,
24 Glass JD (2004) Amyotrophic lateral sclerosis is a distal axonopathy: evidence in mice
25 and man. *Experimental neurology* 185:232-240.
- 26 Frey D, Schneider C, Xu L, Borg J, Spooren W, Caroni P (2000) Early and selective loss of
27 neuromuscular synapse subtypes with low sprouting competence in motoneuron
28 diseases. *The Journal of neuroscience : the official journal of the Society for*
29 *Neuroscience* 20:2534-2542.
- 30 Georgiou J, Robitaille R, Charlton MP (1999) Muscarinic control of cytoskeleton in perisynaptic
31 glia. *The Journal of neuroscience : the official journal of the Society for Neuroscience*
32 19:3836-3846.
- 33 Georgiou J, Robitaille R, Trimble WS, Charlton MP (1994) Synaptic regulation of glial protein
34 expression in vivo. *Neuron* 12:443-455.
- 35 Gonzalez de Aguilar JL, Niederhauser-Wiederkehr C, Halter B, De Tapia M, Di Scala F, Demougin
36 P, Dupuis L, Primig M, Meininger V, Loeffler JP (2008) Gene profiling of skeletal muscle
37 in an amyotrophic lateral sclerosis mouse model. *Physiol Genomics* 32:207-218.
- 38 Haidet-Phillips AM, Hester ME, Miranda CJ, Meyer K, Braun L, Frakes A, Song S, Likhite S,
39 Murtha MJ, Foust KD, Rao M, Eagle A, Kammesheidt A, Christensen A, Mendell JR,
40 Burghes AH, Kaspar BK (2011) Astrocytes from familial and sporadic ALS patients are
41 toxic to motor neurons. *Nat Biotechnol* 29:824-828.
- 42 Hegedus J, Putman CT, Gordon T (2007) Time course of preferential motor unit loss in the SOD1
43 G93A mouse model of amyotrophic lateral sclerosis. *Neurobiology of disease* 28:154-
44 164.

- 1 Hegedus J, Putman CT, Tyreman N, Gordon T (2008) Preferential motor unit loss in the SOD1
2 G93A transgenic mouse model of amyotrophic lateral sclerosis. *J Physiol* 586:3337-3351.
- 3 Henriques A, Pitzer C, Dittgen T, Klugmann M, Dupuis L, Schneider A (2011) CNS-targeted viral
4 delivery of G-CSF in an animal model for ALS: improved efficacy and preservation of the
5 neuromuscular unit. *Mol Ther* 19:284-292.
- 6 Heredia DJ, Feng CY, Hennig GW, Renden RB, Gould TW (2018) Activity-induced Ca(2+) signaling
7 in perisynaptic Schwann cells of the early postnatal mouse is mediated by P2Y1
8 receptors and regulates muscle fatigue. *Elife* 7.
- 9 Ilieva H, Polymenidou M, Cleveland DW (2009) Non-cell autonomous toxicity in
10 neurodegenerative disorders: ALS and beyond. *The Journal of cell biology* 187:761-772.
- 11 Jahromi BS, Robitaille R, Charlton MP (1992) Transmitter release increases intracellular calcium
12 in perisynaptic Schwann cells in situ. *Neuron* 8:1069-1077.
- 13 Kang H, Lichtman JW (2013) Motor axon regeneration and muscle reinnervation in young adult
14 and aged animals. *J Neurosci* 33:19480-19491.
- 15 Kang H, Tian L, Mikesch M, Lichtman JW, Thompson WJ (2014) Terminal Schwann cells
16 participate in neuromuscular synapse remodeling during reinnervation following nerve
17 injury. *J Neurosci* 34:6323-6333.
- 18 Kang SH, Li Y, Fukaya M, Lorenzini I, Cleveland DW, Ostrow LW, Rothstein JD, Bergles DE (2013)
19 Degeneration and impaired regeneration of gray matter oligodendrocytes in
20 amyotrophic lateral sclerosis. *Nat Neurosci* 16:571-579.
- 21 Ko CP, Robitaille R (2015) Perisynaptic Schwann Cells at the Neuromuscular Synapse:
22 Adaptable, Multitasking Glial Cells. *Cold Spring Harb Perspect Biol* 7:a020503.
- 23 Lalancette-Hebert M, Swarup V, Beaulieu JM, Bohacek I, Abdelhamid E, Weng YC, Sato S, Kriz J
24 (2012) Galectin-3 is required for resident microglia activation and proliferation in
25 response to ischemic injury. *The Journal of neuroscience : the official journal of the*
26 *Society for Neuroscience* 32:10383-10395.
- 27 Lerman BJ, Hoffman EP, Sutherland ML, Bouri K, Hsu DK, Liu FT, Rothstein JD, Knoblach SM
28 (2012) Deletion of galectin-3 exacerbates microglial activation and accelerates disease
29 progression and demise in a SOD1(G93A) mouse model of amyotrophic lateral sclerosis.
30 *Brain Behav* 2:563-575.
- 31 Lobsiger CS, Boillee S, McAlonis-Downes M, Khan AM, Feltri ML, Yamanaka K, Cleveland DW
32 (2009) Schwann cells expressing dismutase active mutant SOD1 unexpectedly slow
33 disease progression in ALS mice. *Proceedings of the National Academy of Sciences of the*
34 *United States of America* 106:4465-4470.
- 35 Love FM, Thompson WJ (1999) Glial cells promote muscle reinnervation by responding to
36 activity-dependent postsynaptic signals. *J Neurosci* 19:10390-10396.
- 37 Lucas CA, Kang LH, Hoh JF (2000) Monospecific antibodies against the three mammalian fast
38 limb myosin heavy chains. *Biochem Biophys Res Commun* 272:303-308.
- 39 Martineau E, Di Polo A, Vande Velde C, Robitaille R (2018) Dynamic neuromuscular remodeling
40 precedes motor-unit loss in a mouse model of ALS. *Elife* 7.
- 41 Mesnard NA, Haulcomb MM, Tanzer L, Sanders VM, Jones KJ (2013) Delayed functional
42 recovery in presymptomatic mSOD1 mice following facial nerve crush axotomy. *J*
43 *Neurodegener Regen* 4:21-25.

- 1 Meyer K, Ferraiuolo L, Miranda CJ, Likhite S, McElroy S, Rensch S, Ditsworth D, Lagier-
2 Tourenne C, Smith RA, Ravits J, Burghes AH, Shaw PJ, Cleveland DW, Kolb SJ, Kaspar BK
3 (2014) Direct conversion of patient fibroblasts demonstrates non-cell autonomous
4 toxicity of astrocytes to motor neurons in familial and sporadic ALS. *Proc Natl Acad Sci U*
5 *S A* 111:829-832.
- 6 Morizawa YM, Hirayama Y, Ohno N, Shibata S, Shigetomi E, Sui Y, Nabekura J, Sato K, Okajima F,
7 Takebayashi H, Okano H, Koizumi S (2017) Reactive astrocytes function as phagocytes
8 after brain ischemia via ABCA1-mediated pathway. *Nature communications* 8:28.
- 9 Nguyen JV, Soto I, Kim KY, Bushong EA, Oglesby E, Valiente-Soriano FJ, Yang Z, Davis CH, Bedont
10 JL, Son JL, Wei JO, Buchman VL, Zack DJ, Vidal-Sanz M, Ellisman MH, Marsh-Armstrong N
11 (2011) Myelination transition zone astrocytes are constitutively phagocytic and have
12 synuclein dependent reactivity in glaucoma. *Proc Natl Acad Sci U S A* 108:1176-1181.
- 13 O'Malley JP, Waran MT, Balice-Gordon RJ (1999) In vivo observations of terminal Schwann cells
14 at normal, denervated, and reinnervated mouse neuromuscular junctions. *J Neurobiol*
15 38:270-286.
- 16 Painter MW, Brosius Lutz A, Cheng YC, Latremoliere A, Duong K, Miller CM, Posada S, Cobos EJ,
17 Zhang AX, Wagers AJ, Havton LA, Barres B, Omura T, Woolf CJ (2014) Diminished
18 Schwann cell repair responses underlie age-associated impaired axonal regeneration.
19 *Neuron* 83:331-343.
- 20 Parone PA, Da Cruz S, Han JS, McAlonis-Downes M, Vetto AP, Lee SK, Tseng E, Cleveland DW
21 (2013) Enhancing mitochondrial calcium buffering capacity reduces aggregation of
22 misfolded SOD1 and motor neuron cell death without extending survival in mouse
23 models of inherited amyotrophic lateral sclerosis. *J Neurosci* 33:4657-4671.
- 24 Pun S, Santos AF, Saxena S, Xu L, Caroni P (2006) Selective vulnerability and pruning of phasic
25 motoneuron axons in motoneuron disease alleviated by CNTF. *Nature neuroscience*
26 9:408-419.
- 27 Reichert F, Saada A, Rotshenker S (1994) Peripheral nerve injury induces Schwann cells to
28 express two macrophage phenotypes: phagocytosis and the galactose-specific lectin
29 MAC-2. *The Journal of neuroscience : the official journal of the Society for Neuroscience*
30 14:3231-3245.
- 31 Reynolds ML, Woolf CJ (1992) Terminal Schwann cells elaborate extensive processes following
32 denervation of the motor endplate. *J Neurocytol* 21:50-66.
- 33 Robitaille R (1998) Modulation of synaptic efficacy and synaptic depression by glial cells at the
34 frog neuromuscular junction. *Neuron* 21:847-855.
- 35 Rocha MC, Pousinha PA, Correia AM, Sebastiao AM, Ribeiro JA (2013) Early changes of
36 neuromuscular transmission in the SOD1(G93A) mice model of ALS start long before
37 motor symptoms onset. *PLoS One* 8:e73846.
- 38 Rochon D, Rouse I, Robitaille R (2001) Synapse-glia interactions at the mammalian
39 neuromuscular junction. *The Journal of neuroscience : the official journal of the Society*
40 *for Neuroscience* 21:3819-3829.
- 41 Rotshenker S (2009) The role of Galectin-3/MAC-2 in the activation of the innate-immune
42 function of phagocytosis in microglia in injury and disease. *J Mol Neurosci* 39:99-103.

- 1 Rotshenker S, Reichert F, Gitik M, Haklai R, Elad-Sfadia G, Kloog Y (2008) Galectin-3/MAC-2, Ras
2 and PI3K activate complement receptor-3 and scavenger receptor-AI/II mediated myelin
3 phagocytosis in microglia. *Glia* 56:1607-1613.
- 4 Rouse I, St-Amour A, Darabid H, Robitaille R (2010) Synapse-glia interactions are governed by
5 synaptic and intrinsic glial properties. *Neuroscience* 167:621-632.
- 6 Schaefer AM, Sanes JR, Lichtman JW (2005) A compensatory subpopulation of motor neurons in
7 a mouse model of amyotrophic lateral sclerosis. *The Journal of comparative neurology*
8 490:209-219.
- 9 Schiaffino S, Gorza L, Sartore S, Saggin L, Ausoni S, Vianello M, Gundersen K, Lomo T (1989)
10 Three myosin heavy chain isoforms in type 2 skeletal muscle fibres. *J Muscle Res Cell*
11 *Motil* 10:197-205.
- 12 Shahidullah M, Le Marchand SJ, Fei H, Zhang J, Pandey UB, Dalva MB, Pasinelli P, Levitan IB
13 (2013) Defects in synapse structure and function precede motor neuron degeneration in
14 *Drosophila* models of FUS-related ALS. *J Neurosci* 33:19590-19598.
- 15 Sharp PS, Dick JR, Greensmith L (2005) The effect of peripheral nerve injury on disease
16 progression in the SOD1(G93A) mouse model of amyotrophic lateral sclerosis.
17 *Neuroscience* 130:897-910.
- 18 Son YJ, Thompson WJ (1995a) Schwann cell processes guide regeneration of peripheral axons.
19 *Neuron* 14:125-132.
- 20 Son YJ, Thompson WJ (1995b) Nerve sprouting in muscle is induced and guided by processes
21 extended by Schwann cells. *Neuron* 14:133-141.
- 22 Son YJ, Trachtenberg JT, Thompson WJ (1996) Schwann cells induce and guide sprouting and
23 reinnervation of neuromuscular junctions. *Trends in neurosciences* 19:280-285.
- 24 Swarup V, Audet JN, Phaneuf D, Kriz J, Julien JP (2012) Abnormal regenerative responses and
25 impaired axonal outgrowth after nerve crush in TDP-43 transgenic mouse models of
26 amyotrophic lateral sclerosis. *The Journal of neuroscience : the official journal of the*
27 *Society for Neuroscience* 32:18186-18195.
- 28 Tallon C, Russell KA, Sakhalkar S, Andrapallayal N, Farah MH (2016) Length-dependent axo-
29 terminal degeneration at the neuromuscular synapses of type II muscle in SOD1 mice.
30 *Neuroscience* 312:179-189.
- 31 Thompson W, Jansen JK (1977) The extent of sprouting of remaining motor units in partly
32 denervated immature and adult rat soleus muscle. *Neuroscience* 2:523-535.
- 33 Todd KJ, Darabid H, Robitaille R (2010) Perisynaptic glia discriminate patterns of motor nerve
34 activity and influence plasticity at the neuromuscular junction. *The Journal of*
35 *neuroscience : the official journal of the Society for Neuroscience* 30:11870-11882.
- 36 Tremblay E, Martineau E, Robitaille R (2017) Opposite Synaptic Alterations at the
37 Neuromuscular Junction in an ALS Mouse Model: When Motor Units Matter. *J Neurosci*
38 37:8901-8918.
- 39 Turner BJ, Ackerley S, Davies KE, Talbot K (2010) Dismutase-competent SOD1 mutant
40 accumulation in myelinating Schwann cells is not detrimental to normal or transgenic
41 ALS model mice. *Human molecular genetics* 19:815-824.
- 42 Valdez G, Tapia JC, Lichtman JW, Fox MA, Sanes JR (2012) Shared resistance to aging and ALS in
43 neuromuscular junctions of specific muscles. *PLoS one* 7:e34640.

- 1 Van Dyke JM, Smit-Oistad IM, Macrander C, Krakora D, Meyer MG, Suzuki M (2016)
2 Macrophage-mediated inflammation and glial response in the skeletal muscle of a rat
3 model of familial amyotrophic lateral sclerosis (ALS). *Exp Neurol* 277:275-282.
- 4 Wang L, Pytel P, Feltri ML, Wrabetz L, Roos RP (2012) Selective knockdown of mutant SOD1 in
5 Schwann cells ameliorates disease in G85R mutant SOD1 transgenic mice. *Neurobiol Dis*
6 48:52-57.
- 7 Wright MC, Potluri S, Wang X, Dentcheva E, Gautam D, Tessler A, Wess J, Rich MM, Son YJ
8 (2009) Distinct muscarinic acetylcholine receptor subtypes contribute to stability and
9 growth, but not compensatory plasticity, of neuromuscular synapses. *The Journal of*
10 *neuroscience : the official journal of the Society for Neuroscience* 29:14942-14955.
- 11 Wyatt RM, Balice-Gordon RJ (2008) Heterogeneity in synaptic vesicle release at neuromuscular
12 synapses of mice expressing synaptopHluorin. *J Neurosci* 28:325-335.
- 13 Yamanaka K, Chun SJ, Boillee S, Fujimori-Tonou N, Yamashita H, Gutmann DH, Takahashi R,
14 Misawa H, Cleveland DW (2008) Astrocytes as determinants of disease progression in
15 inherited amyotrophic lateral sclerosis. *Nature neuroscience* 11:251-253.
- 16 Yang RY, Rabinovich GA, Liu FT (2008) Galectins: structure, function and therapeutic potential.
17 *Expert Rev Mol Med* 10:e17.
- 18 Zhou JY, Afjehi-Sadat L, Asress S, Duong DM, Cudkowicz M, Glass JD, Peng J (2010) Galectin-3 is
19 a candidate biomarker for amyotrophic lateral sclerosis: discovery by a proteomics
20 approach. *J Proteome Res* 9:5133-5141.
- 21 Zwieggers P, Lee G, Shaw CA (2014) Reduction in hSOD1 copy number significantly impacts ALS
22 phenotype presentation in G37R (line 29) mice: implications for the assessment of
23 putative therapeutic agents. *J Negat Results Biomed* 13:14.

24